PHYSICAL REVIEW D **88,** 065024 (2013)

Neutrino spectral density at electroweak scale temperature

Kohtaroh Miura,[1,*] Yoshimasa Hidaka,[2,†] Daisuke Satow,[2,3,‡] and Teiji Kunihiro[3,§]

[1]*INFN-Laboratori Nazionali di Frascati, I-00044 Frascati(RM), Italy*
[2]*Theoretical Research Division, Nishina Center, RIKEN, Wako 351-0198, Japan*
[3]*Department of Physics, Kyoto University, Kyoto 606-8502, Japan*

(Received 28 June 2013; published 23 September 2013)

Motivated by the scenario of resonant leptogenesis in which lepton number creation in the electroweak scale is relevant, we investigate the spectral properties and possible collective nature of the standard model neutrinos at electroweak scale temperature (T). We adopt the R_ξ gauge fixing, which includes the unitary gauge as a limiting case, and allows us to study the broken as well as the restored phases of the gauge symmetry in a unified way. We show that the spectral density of the neutrino has a three-peak structure in the low-momentum region due to the scattering with the thermally excited particles (i.e., Landau damping) for $T \gtrsim M_{\mathrm{W,Z}}(T)$, with $M_{\mathrm{W,Z}}(T)$ being the weak-boson masses in the plasma. The three peaks are identified with a novel ultrasoft mode, the usual quasiparticle, and antiplasmino modes. Varying the gauge-fixing parameter ξ, we show that the three-peak structure appears independently of the gauge fixing and thus has a physical significance. We discuss possible implications of the neutrino spectral density obtained in the present work on particle cosmology, in particular in the context of resonant leptogenesis.

DOI: 10.1103/PhysRevD.88.065024 PACS numbers: 11.10.Wx, 11.15.Ex, 12.15.−y, 13.15.+g

I. INTRODUCTION

Thermodynamic properties of gauge theories are of common interest in various fields of physics [1,2], including baryogenesis and leptogenesis, the physics of quark-gluon plasma (QGP), neutrino physics in big-bang nucleosynthesis and in compact stars, and many others. A novel ingredient in the dynamics at finite temperature (T) is due to the existence of thermally excited particles, with which a probe particle is scattered in the classical level, leading to a damping known as Landau damping and a modification of the spectral properties of the probe particle. In this paper, partly motivated by the recent development of the resonant leptogenesis scenario [3,4], we study the spectral properties of neutrinos at finite T, specifically in the electroweak scale, in a way where the gauge (in)dependence is manifestly checked.

Although the standard model (SM) seems to fail to explain the observed baryon asymmetry of the universe (BAU), an extension of the SM by adding right-handed Majorana neutrinos (N_{R}) may have a chance to account for the BAU. Indeed, a thermal leptogenesis scenario based on such an extended model [5,6] gives a simple and promising account of the BAU. In this scenario, a decay of N_{R} out of equilibrium via Yukawa interactions generates a net lepton number, which is partially converted into the baryon numbers through sphaleron processes [7–9] in the electroweak phase transition. Furthermore, if the mass difference between two right-handed neutrinos is on the order of their CP-violating decay width, the CP asymmetry is dynamically enhanced and so is leptogenesis [3,4]. This resonant leptogenesis scenario implies that N_{R} with a TeV-scale or electroweak-scale mass is relevant to the BAU and thus has opened a possibility to create a lepton number at electroweak scale temperature.

Figure 1 shows the CP-violating decay process of N_{R}, which gives one of the most important contributions to lepton number creation, where both the Higgs particle and leptons are involved. In the present work, we suppose that the relevant processes occur at finite T of the electroweak scale. In this T region, the following two finite-T effects come into play: 1) the Landau damping of the Higgs particle and leptons by thermally excited particles including massive gauge bosons; 2) the T dependence of the masses of the involved particles, generated by the Englert-Brout-Higgs-Guralnik-Hagen-Kibble mechanism [10], which will be called simply the Higgs mechanism from now on in this paper. If the standard model leptons have nontrivial spectral properties due to the aforementioned two effects, lepton number creation via the N_{R} decay in Fig. 1 will be significantly modified.

The important role of the Landau damping for modifying the fermion spectral properties is known and established in QED and QCD in the context of QGP physics. A fermion interacting with thermally excited gauge bosons and

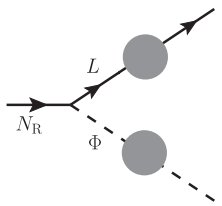

FIG. 1. A decay process of a right-handed Majorana neutrino (N_{R}).

*miura@kmi.nagoya-u.ac.jp
†hidaka@riken.jp
‡daisuke.sato@riken.jp
§kunihiro@ruby.scphys.kyoto-u.ac.jp

antifermions admits a novel collective excitation mode known as a (an anti)plasmino as well as the normal quasiparticle excitation with thermal mass [11]. Such collective excitations in the QGP at extremely high T are shown to exist and their dispersion relations are obtained in a gauge-invariant way, at least at one-loop order, which is now known as the hard thermal loop (HTL) approximation [12]. A full spectral property beyond the dispersion relations of massive electrons in QED plasma is investigated in Ref. [13], where a physical account of the interplay between the electron-mass and temperature-effects that leads to a Landau damping were presented.

As first discussed in Ref. [14], we expect that the leptons appearing in Fig. 1 should also admit nontrivial collective excitations at finite T. Recently, the neutrino spectral properties at electroweak scale temperature in the broken phase have been investigated by using the HTL approximation in the unitary gauge [15]. A remarkable finding there was the possible existence of a novel branch of the dispersion relation with a collective nature in the ultrasoft-energy region. Here, an important question is whether such an ultrasoft mode is physically significant with regards to the gauge invariance, which cannot be checked within the unitary gauge. In fact, the gauge (in)dependence of the spectral properties of neutrinos in the ultrasoft-energy region has not been fully investigated yet, except for those at $T = 1$–10 MeV [14].

Here, we note that the gauge (in)dependence of the spectral properties of massless fermions (quarks) in the ultrasoft-energy region has been discussed in the physics of QGP. It was shown [16,17] that the spectral function of massless quarks coupled to massive vector soft modes in QGP can have a novel peak in the ultrasoft-energy region as well as those corresponding to the normal and the antiplasmino modes, and it was later demonstrated [18] that their properties are gauge independent by using the Stueckelberg formalism [19,20].

Now, one should recognize that the relevant ingredients for the description of hot neutrinos at the electroweak scale temperature are the same as those in Ref. [18], i.e., a massless fermion and a massive vector boson with a mass comparable with T. Thus, a natural and intriguing question is whether the neutrino spectral density at T of the electroweak scale should also develop a three-peak or three-bump structure including an ultrasoft mode without gauge dependence, as quarks do in the QGP [16–18,21–23].

In the present work, we investigate in a gauge-invariant way the spectral properties of neutrinos at weak coupling, without restricting ourselves to their dispersion relations, in the full energy-momentum plane at finite T around the electroweak scale. We show that the neutrino develops an ultrasoft excitation mode as well as the normal and plasmino ones without recourse to the HTL approximation. We shall employ the R_ξ gauge [24] for examining the possible gauge-fixing dependence of the spectral density in both broken and symmetric phases. Furthermore, we also discuss the implications of the resulting neutrino spectral properties to the cosmology by considering electroweak-scale resonant leptogenesis.

This paper is organized as follows. In the next section, we introduce the Lagrangian of the electroweak theory in the R_ξ gauge [24] and the basic quantities to evaluate the spectral properties of neutrinos in field theory at finite temperature. In Sec. III, we show the numerical results for the self-energy and the spectral density of neutrinos in the broken phase. The results will be compared with the unitary-gauge HTL results [15]. In Sec. IV, we extend our study into the symmetric phase, and investigate the fate of collective modes for neutrinos. Then in Sec. V, we discuss possible implications of the neutrino spectral density obtained in the present work in the context of resonant leptogenesis. Finally, we make concluding remarks in Sec. VI. Appendices A, B, C, D, E, and F are devoted to explaining technical details.

II. PRELIMINARIES

A. Electroweak theory at finite temperature in R_ξ gauge

The Lagrangian to be considered is composed of the lepton L, the Higgs Φ, and the gauge boson $\mathcal{G}_\mu = \mathcal{A}_\mu$, $\mathcal{B}_\mu$ sectors,

$$\mathcal{L}[\Phi, L, \mathcal{G}_\mu] = \mathcal{L}_{\rm L}[L, \mathcal{G}_\mu] + \mathcal{L}_{\rm H}[\Phi, \mathcal{G}_\mu] + \mathcal{L}_{\rm G}[\mathcal{G}_\mu], \quad (1)$$

up to gauge fixing and Faddeev-Popov ghost terms. The Higgs sector is given by

$$\mathcal{L}_{\rm H} = (\mathcal{D}_\mu\Phi)^\dagger(\mathcal{D}^\mu\Phi) + \mu_0^2\Phi^\dagger\Phi - \lambda(\Phi^\dagger\Phi)^2, \quad (2)$$

$$\mathcal{D}_\mu\Phi = \left(\partial_\mu\mathbf{1} - ig\frac{\sigma^a\mathcal{A}_\mu^a}{2} - \frac{ig'}{2}\mathcal{B}_\mu\mathbf{1}\right)\Phi, \quad (3)$$

where $\sigma^{a=1,2,3}$ are Pauli matrices, and $\mathcal{A}_\mu$ and $\mathcal{B}_\mu$ are the gauge fields of the $\mathrm{SU_W}(2)$ and $\mathrm{U_Y}(1)$ groups, respectively. The field Φ represents the weak doublet scalar, which can be parametrized as

$$\Phi(x) = \frac{1}{\sqrt{2}}\begin{bmatrix} \phi^2(x) + i\phi^1(x) \\ v + h(x) - i\phi^3(x) \end{bmatrix}. \quad (4)$$

Here, the constant v represents the vacuum expectation value (VEV). The fluctuations of the Higgs field and the Nambu-Goldstone modes are denoted by $h(x)$ and $\phi^a(x)$, respectively, the latter of which is to be eaten by the gauge fields.

The gauge-fixing term in the R_ξ gauge reads

$$\mathcal{L}_{\rm GF} = -\frac{1}{2\xi}((F_{\rm A}^a(x))^2 + (F_{\rm B}(x))^2), \quad (5)$$

where

$$F^a_{\rm A}(x) = \partial_\mu \mathcal{A}^{\mu,a}(x) + \xi m_{\rm A}\phi^a(x), \tag{6}$$

$$F_{\rm B}(x) = \partial_\mu \mathcal{B}^{\mu}(x) - \xi m_{\rm B}\phi^3(x), \tag{7}$$

with $(m_{\rm A}, m_{\rm B}) = (g\mu_0/(2\sqrt{\lambda}), g'\mu_0/(2\sqrt{\lambda}))$. The gauge-fixing conditions are specified by the parameter ξ.

From the gauge-boson sector $\mathcal{L}_{\rm G}$ and the gauge-fixing term $\mathcal{L}_{\rm GF}$, the bare propagators of the gauge bosons are obtained as a sum of the unitary gauge and the ξ-dependent parts,

$$G_{\mu\nu}(q) = G^{\rm U}_{\mu\nu}(q) + G^{\xi}_{\mu\nu}(q), \tag{8}$$

$$G^{\rm U}_{\mu\nu}(q) = -\sum_{t=\pm}\frac{t(g_{\mu\nu} - q_\mu q_\nu/M^2(T))}{2E_{\mathbf{q}}(M)(q_0 - tE_{\mathbf{q}}(M))}, \tag{9}$$

$$G^{\xi}_{\mu\nu}(q) = \sum_{t=\pm}\frac{t\cdot q_\mu q_\nu/M^2(T)}{2E^{\xi}_{\mathbf{q}}(M)(q_0 - tE^{\xi}_{\mathbf{q}}(M))}, \tag{10}$$

where

$$E_{\mathbf{q}}(M) \equiv \sqrt{|\mathbf{q}|^2 + M^2(T)}, \qquad E^{\xi}_{\mathbf{q}}(M) \equiv E_{\mathbf{q}}(\sqrt{\xi}M), \tag{11}$$

and $M(T)$ represents the W boson, Z boson, or photon mass at finite T: $M(T) = M_{\rm W}(T)$, $M_{\rm Z}(T)$, $M_{\rm ph}(T)$. In the weak coupling, the weak-boson masses $M_{\rm W,Z}(T)$ at finite temperature are given by simply replacing the VEV at the vacuum ($v_0 = \mu_0/\sqrt{\lambda} = 246$ GeV) with that at finite temperature $v(T)$,

$$(M_{\rm W}(T), M_{\rm Z}(T), M_{\rm ph}(T)) = \left(\frac{gv(T)}{2}, \frac{\sqrt{g^2+g'^2}v(T)}{2}, 0\right). \tag{12}$$

In fact, the weak-boson masses (12) acquire thermal corrections of order gT from the one-loop self-energy, as was shown by C. Manuel [25] under the condition $M_{\rm W,Z}(T) \ll T$ and $\lambda \to \infty$ in the Stueckelberg formalism. However, our main focus is on the region satisfying $M_{\rm W,Z} \sim gv(T) \gg gT$, or equivalently $v(T) \gg T$, which means that the thermal corrections to the masses are of higher order at weak coupling, and can be neglected in the region of our interest.

Next, we discuss how to choose the effective potential in the Higgs sector. The lattice Monte Carlo simulations have shown that the electroweak symmetry breaking or restoration is a smooth crossover [26] for a Higgs mass $m_{\rm H}$ larger than about ~70 GeV in the standard model. Assuming that the new boson with the mass around 125–127 GeV observed at the LHC [27–30] is the Higgs particle, the possibility of a strong first-order electroweak transition is excluded within the standard model. Note that a strong first-order electroweak transition is not necessary in the thermal leptogenesis scenario, unlike some other scenarios of baryon number creation [31]. As pointed out in Ref. [15], the absence of the first-order transition indicates that the weak-boson masses in electroweak plasma $M_{\rm W,Z}(T)$ smoothly go to zero. Therefore, there should exist a temperature regime satisfying $M_{\rm W,Z}(T) \sim T$, where we expect a nontrivial spectral property of the standard model particles. In order to implement this feature with a smooth transition, we use the following Higgs effective potential [2]:

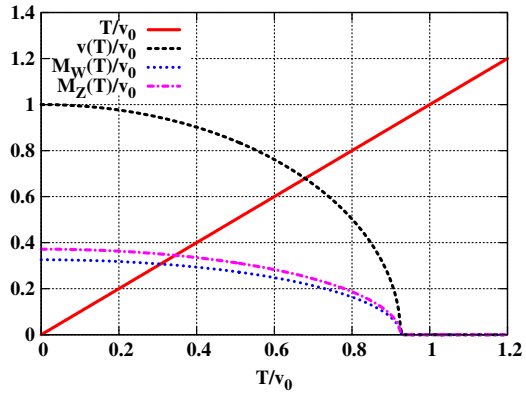

FIG. 2 (color online). The VEV and gauge-boson masses in thermal background as a function of temperature T. All quantities are normalized by the vacuum VEV $v_0 = 246$ GeV.

$$V_{\rm eff} = -\frac{1}{2}\mu^2(T)v^2(T) + \frac{\lambda}{4}v^4(T), \tag{13}$$

$$\mu^2(T) = \mu_0^2\left(1 - \frac{T^2}{T_c^2}\right), \tag{14}$$

$$T_c^2 = \frac{4\mu_0^2}{2\lambda + 3g^2/4 + g'^2/4}, \tag{15}$$

where $\mu_0^2 = m_{\rm H}^2/2$ and $\lambda = m_{\rm H}^2/(2v_0^2)$ are the mass and coupling parameters in the Higgs Lagrangian (2). This effective potential has been derived in the R_ξ gauge by taking account of the leading order of the high-T expansion for thermal one-loop effects of the Higgs and gauge bosons in addition to the tree-level Higgs potential. The ξ dependencies cancel out between the Nambu-Goldstone bosons and the ghost contributions. The effective potential leads to the second-order phase transition, and the VEV at finite T is obtained as

$$v^2(T) = v_0^2\left(1 - \frac{T^2}{T_c^2}\right), \qquad T \le T_c. \tag{16}$$

Figure 2 shows the $v(T)$ and the weak-boson masses as a function of temperature.

B. Self-energy and spectral density for left-handed neutrinos at finite T

In the broken phase of the electroweak symmetry, the Lagrangian for the lepton sector takes the following form:

$$\mathcal{L}_{\mathrm{L}} = \sum_{i=e,\mu,\tau}\left[(\bar{\nu}^i, \bar{l}^i_{\mathrm{L}})i\partial\!\!\!/\begin{pmatrix}\nu^i\\ l^i_{\mathrm{L}}\end{pmatrix} + \bar{l}^i_{\mathrm{R}}i\partial\!\!\!/ l^i_{\mathrm{R}}\right] + (W^\dagger_\mu J^\mu_{\mathrm{W}} + J^\dagger_{\mathrm{W}\mu}W^\mu + Z_\mu J^\mu_{\mathrm{Z}} + A^{\mathrm{EM}}_\mu J^\mu_{\mathrm{EM}}), \tag{17}$$

where $\nu^i = \mathcal{P}_{\mathrm{L}}\nu^i_{\mathrm{D}}$ and $l^i_{\mathrm{L/R}} = \mathcal{P}_{\mathrm{L/R}}l^i$ represent the left-handed neutrinos and left-handed (right-handed) charged leptons, respectively. Since we are interested in the temperature region comparable to the weak-boson masses $T \sim M_{\mathrm{W,Z}}(T)$, where the lepton masses are much smaller than $M_{\mathrm{W,Z}}(T)$, we have neglected such tiny masses of the leptons. It is expected that the massless approximation will not affect the basic spectral properties of the neutrinos, as is demonstrated in the case of light quarks in QGP [17,32].

The gauge currents in the Lagrangian (17) are found to be

$$J^\mu_{\mathrm{W}} = \frac{g}{\sqrt{2}}\sum_{i=e,\mu,\tau}\bar{l}^i\gamma^\mu\mathcal{P}_{\mathrm{L}}\nu^i_{\mathrm{D}}, \tag{18}$$

$$J^\mu_{\mathrm{Z}} = \sum_{i=e,\mu,\tau}\left[\frac{g\sin^2\theta_w}{\cos\theta_w}\bar{l}^i\gamma^\mu l^i + \frac{g}{\cos\theta_w}(\bar{\nu}^i_{\mathrm{D}}, \bar{l}^i)\times\mathcal{P}_{\mathrm{R}}\gamma^\mu\mathcal{P}_{\mathrm{L}}\frac{\sigma^3}{2}\begin{pmatrix}\nu^i_{\mathrm{D}}\\ l^i\end{pmatrix}\right], \tag{19}$$

$$J^\mu_{\mathrm{EM}} = -e\sum_{i=e,\mu,\tau}\bar{l}^i\gamma^\mu l^i, \tag{20}$$

where the couplings g, g', e and the Weinberg angle θ_w are given in Table I in Appendix A. The Feynman diagram for the neutrino self-energy is shown in Fig. 3. We note that a neutral-current tadpole diagram with a lepton loop does not appear in the CP-symmetric thermal background, which we assume because we are motivated by the scenario of thermal leptogenesis, where the CP violation is considered to arise from the decay of right-handed neutrinos rather than the thermal background itself. For the massless neutrinos, it is sufficient to consider the single-generation case, and thus we drop the generation index "i."

The Feynman diagrams listed in Fig. 3 include the following one-loop integral as a common factor:

$$\sigma(\mathbf{p}, i\omega_m; T, M(T)) = T\sum_n\int\frac{d^3k}{(2\pi)^3}(-i\gamma^\mu)G_{\mathrm{F}}(\mathbf{k}, \omega_n)\times(-i\gamma^\nu)G_{\mu\nu}(\mathbf{p}-\mathbf{k}, i\omega_m - i\omega_n), \tag{21}$$

where G_{F} represents an imaginary-time propagator for a lepton. Self-energy corrections in G_{F} are of order g^2T and can be neglected at weak coupling. Accordingly, we can use the massless propagator as G_{F},

$$G_{\mathrm{F}}(\mathbf{k}, \omega_n) = \frac{i}{i\omega_n\gamma^0 - \mathbf{k}\cdot\boldsymbol{\gamma}} = \sum_{s=\pm}\frac{\Lambda_{\mathbf{k},s}\gamma^0}{i\omega_n - s|\mathbf{k}|}, \tag{22}$$

with

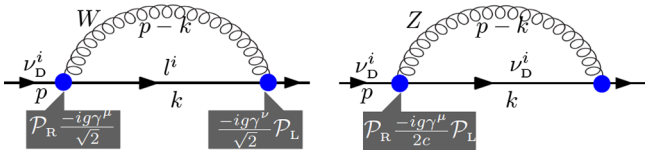

FIG. 3 (color online). One-loop Feynman diagrams of the neutrino self-energies with the weak-boson exchanges. The symbols "l^i" and "ν^i_{D}" represent a charged lepton and a Dirac neutrino in the "ith" generation, respectively. The oriented lines represent a fermion propagator. The chirality is managed by the projection operators $\mathcal{P}_{\mathrm{L/R}} = (1 \mp \gamma_5)/2$ on the vertex. In the right panel, $c = \cos\theta_w$.

$$\Lambda_{\pm,\mathbf{k}} = \frac{1 \pm \gamma^0\hat{\mathbf{k}}\cdot\boldsymbol{\gamma}}{2}, \qquad \hat{\mathbf{k}} = \mathbf{k}/|\mathbf{k}|. \tag{23}$$

The weak-boson propagator $G_{\mu\nu}$ is given by Eq. (8) with the momentum identification $q_\mu = (i\omega_m - i\omega_n, \mathbf{p}-\mathbf{k})$, and the mass $M(T)$ is interpreted to be the W or Z mass shown in Eq. (12). We note that the projection operator $\mathcal{P}_{\mathrm{L/R}}$ has not been included in Eq. (21), and will be taken account of later.

The nontrivial thermal effect emerges from the one-loop momentum integral in the self-energy (21), and we evaluate it in the imaginary-time formalism. Carrying out the summation over the Matsubara frequency n and applying the analytic continuation $i\omega_m \to \omega + i\eta$ in Eq. (21), we obtain the retarded self-energy as

$$\sigma^{\mathrm{ret}}(\mathbf{p}, \omega; T, M) = \sigma^{\mathrm{ret}}_{\mathrm{U}}(\mathbf{p}, \omega; T, M) + \sigma^{\mathrm{ret}}_{\xi}(\mathbf{p}, \omega; T, M), \tag{24}$$

where

$$\sigma^{\mathrm{ret}}_{\mathrm{U}}(\mathbf{p}, \omega; T, M) = -\sum_{s,t=\pm}\int\frac{d^3k}{(2\pi)^3}\frac{t\gamma^\mu\Lambda_{s,\mathbf{k}}\gamma^0\gamma^\nu}{2E_{\mathbf{q}}}\times\left(g_{\mu\nu} - \frac{q_\mu q_\nu}{M^2(T)}\right)\times\frac{N_{\mathrm{F}}(s|\mathbf{k}|/T) + N_{\mathrm{B}}(-tE_{\mathbf{q}}/T)}{\omega - s|\mathbf{k}| - tE_{\mathbf{q}}(M) + i\eta}, \tag{25}$$

$$\sigma^{\mathrm{ret}}_{\xi}(\mathbf{p}, \omega; T, M) = -\sum_{s,t=\pm}\int\frac{d^3k}{(2\pi)^3}\frac{t\gamma^\mu\Lambda_{s,\mathbf{k}}\gamma^0\gamma^\nu}{2E^\xi_{\mathbf{q}}(M)}\times\frac{N_{\mathrm{F}}(s|\mathbf{k}|/T) + N_{\mathrm{B}}(-tE^\xi_{\mathbf{q}}/T)}{\omega - s|\mathbf{k}| - tE^\xi_{\mathbf{q}}(M) + i\eta}. \tag{26}$$

Here, the indices "U" and "ξ" are associated with the unitary gauge and the ξ-dependent gauge-boson propagators defined in Eqs. (8)–(10). The gauge-boson energy $E_{\mathbf{q}}$ is defined in Eq. (11), and $N_{\mathrm{F,B}}$ represent the Fermi-Dirac and Bose-Einstein distribution functions, respectively,

$$N_{\mathrm{F}}(x) = \frac{1}{e^x + 1}, \qquad N_{\mathrm{B}}(x) = \frac{1}{e^x - 1}. \tag{27}$$

Similarly to the propagator G_{F}, we decompose the retarded self-energy σ^{ret} as

$$\sigma^{\rm ret}(\mathbf{p},\omega;T,M(T)) = \sum_{s=\pm}[\Lambda_{s,\mathbf{p}}\gamma^0]\sigma_s(\mathbf{p},\omega;T,M(T)), \quad (28)$$

where the coefficients

$$\sigma_\pm(\mathbf{p},\omega;T,M(T)) = \frac{1}{2}\,{\rm tr}_{\rm spin}\left[\Sigma^{\rm ret}(\mathbf{p},\omega;T)\Lambda_{\pm,\mathbf{p}}\gamma^0\right] \quad (29)$$

are responsible for finite-T effects. By using $\sigma_\pm$, the retarded self-energy for the left-handed neutrinos $\Sigma^{(\nu)}_{\rm ret}$ is now constructed as

$$\Sigma^{(\nu)}_{\rm ret}(\mathbf{p},\omega;T) = \sum_{s=\pm}[\mathcal{P}_{\rm R}\Lambda_{s,\mathbf{p}}\gamma^0\mathcal{P}_{\rm L}]\Sigma^{(\nu)}_s(|\mathbf{p}|,\omega;T), \quad (30)$$

where

$$\Sigma^{(\nu)}_\pm(|\mathbf{p}|,\omega;T) = \left(\frac{g}{\sqrt{2}}\right)^2\sigma_\pm(|\mathbf{p}|,\omega;T,M_{\rm W}(T)) + \left(\frac{g}{2\cos\theta_w}\right)^2\sigma_\pm(|\mathbf{p}|,\omega;T,M_{\rm Z}(T)), \quad (31)$$

as read off from the structure of the chirality and the gauge interaction given by Eqs. (17)–(20) (and Fig. 3). In Eq. (30), the left-handed nature of massless neutrinos is taken care of by the spinor matrix $\mathcal{P}_{\rm L}\Lambda_{\pm,\mathbf{p}}\gamma^0\mathcal{P}_{\rm R}$.

We shall now investigate the neutrino spectral density, which is defined by the imaginary part of the retarded Green function,

$$\rho^{(\nu)}(\mathbf{p},\omega;T) = \sum_{s=\pm}[\mathcal{P}_{\rm R}\Lambda_{s,\mathbf{p}}\gamma^0\mathcal{P}_{\rm L}]\rho^{(\nu)}_s(|\mathbf{p}|,\omega;T) \equiv -\frac{1}{\pi}\,{\rm Im}G^{(\nu)}_{\rm ret}(\mathbf{p},\omega;T), \quad (32)$$

where

$$G^{(\nu)}_{\rm ret}(\mathbf{p},\omega;T) = \sum_{s=\pm}\frac{\mathcal{P}_{\rm R}\Lambda_{s,\mathbf{p}}\gamma^0\mathcal{P}_{\rm L}}{(\omega+i\eta)-s|\mathbf{p}|-\Sigma^{(\nu)}_s(|\mathbf{p}|,\omega;T)}, \quad (33)$$

or equivalently,

$$\rho^{(\nu)}_\pm(|\mathbf{p}|,\omega;T) = \frac{-{\rm Im}\Sigma^{(\nu)}_\pm(|\mathbf{p}|,\omega;T,\xi)/\pi}{\{\mathcal{D}^{(\nu)}_\pm(|\mathbf{p}|,\omega;T,\xi)\}^2+\{{\rm Im}\Sigma^{(\nu)}_\pm(|\mathbf{p}|,\omega;T,\xi)\}^2}, \quad (34)$$

$$\mathcal{D}^{(\nu)}_\pm(|\mathbf{p}|,\omega;T,\xi) = \omega-|\mathbf{p}|\mp{\rm Re}\Sigma^{(\nu)}_\pm(|\mathbf{p}|,\omega;T,\xi). \quad (35)$$

The calculational procedure of ${\rm Im}\Sigma^{(\nu)}_\pm$ and ${\rm Re}\Sigma^{(\nu)}_\pm$ is summarized in Appendix C.

Note that finite-T effects on the spectral density $\rho^{(\nu)}$ of the left-handed neutrino are solely encoded in the spectral densities $\rho^{(\nu)}_\pm(|\mathbf{p}|,\omega;T)$ appearing as coefficients in the decomposition (32). Thus, our focus will be put on the spectral densities $\rho^{(\nu)}_\pm(|\mathbf{p}|,\omega;T)$ defined in Eq. (34). Similarly, the thermal effects for the spectral density of the massless charged lepton are calculable without the complication of the Dirac spinor structure.

Equations (31) and (34) show that the computation of the neutrino spectral density $\rho^{(\nu)}_\pm(|\mathbf{p}|,\omega;T)$ is reduced to that of the self-energy $\sigma_\pm$ defined in Eq. (29). Fortunately, this task is essentially the same as that of the self-energy of the quark coupled with massive bosonic excitations in a QGP, and this been carried out in a series of papers [16–18]. Therefore, we here omit the technical details but recapitulate them with adequate modifications for the present context in Appendices B and C.

III. NEUTRINO SPECTRAL DENSITY: NUMERICAL RESULTS

In this section, we show our main results for the self-energy and the spectral density of the massless left-handed neutrinos. In Sec. III A, we present $\rho^{(\nu)}_+$ defined in Eq. (34) in the ω-$|\mathbf{p}|$ plane at various temperatures in 't Hooft-Feynman gauge ($\xi = 1$), and show that the neutrino spectral density has a three-peak structure in the low-energy and low-momentum region when the gauge-boson mass $M_{\rm W,Z}$ is comparable to T. Next, in Sec. III B we analyze the three-peak structure in detail and the novel low-lying collective mode for $\xi = 1$. Finally, we examine the ξ dependence of the collective modes in Sec. III C. We clarify the relation between the present results and those obtained in the previous work [15], where the HTL approximation is used and the unitary gauge is adopted. All results have been obtained by using the values in Table I in Appendix A.

A. Neutrino spectral density in the ω-$|\mathbf{p}|$ plane

In Fig. 4, we show the neutrino spectral density $\rho^{(\nu)}_+(|\mathbf{p}|,\omega;T)$ in the ω-$|\mathbf{p}|$ plane at temperatures $T/v_0 = 0.2$, 0.5, and 0.8. Throughout this paper, we do not analyze $\rho^{(\nu)}_-$ because that quantity can be calculated from $\rho^{(\nu)}_+$ due to the particle-antiparticle symmetry [16]. In the $T/v_0 = 0.2$ case (left panel), the spectral density has sharp and narrow peaks almost on the light cone, $\omega = |\mathbf{p}|$. As shown in Fig. 2, the weak-boson masses at $T/v_0 = 0.2$ are still larger than the temperature, $M_{\rm W}/T \simeq 1.59$, for which the effects of thermal excitations [Eqs. (B10) and (B11)] are exponentially suppressed. As a result, the general property of the spectral density at this temperature region is similar to that of a massless particle at zero temperature.

This feature drastically changes when T reaches around $T/v_0 \sim 0.35$, where the weak-boson masses become comparable to T, as is seen in Fig. 2. At this intermediate temperature regime ($T \gtrsim M_{\rm W,Z}$), the weak bosons become thermally excited with a considerable probability. The middle panel of Fig. 4 shows the spectral density $\rho^{(\nu)}_+$ at $T/v_0 = 0.5$, a typical example at intermediate temperature. We see that a three-peak structure is realized in the low-energy and low-momentum region: the three peaks

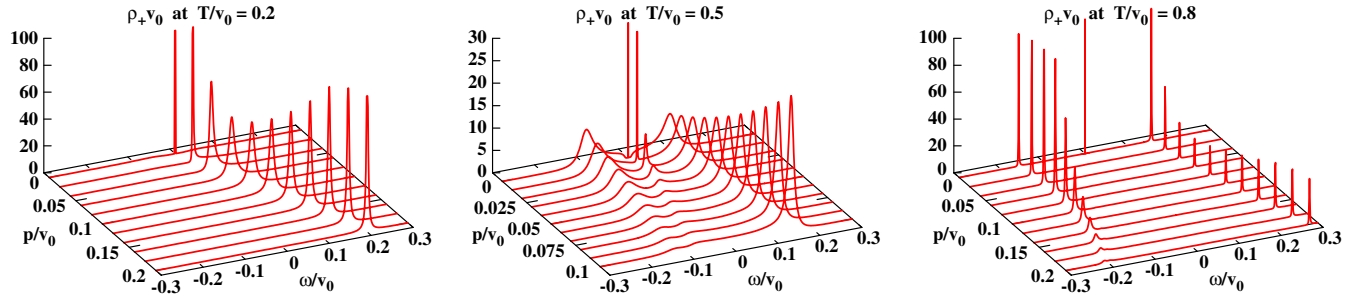

FIG. 4 (color online). The momentum evolution of the spectral density $\rho_+^{(\nu)} v_0$ at $T/v_0 = 0.2$ (left), 0.5 (middle), and 0.8 (right).

consist of two peaks in the positive- and negative-energy regions and the sharp peak around the origin, whose dispersion relations are quite different from that for the free massless particle and are interpreted as collective excitations. As the momentum $|\mathbf{p}|$ increases, the peak in the positive-energy region becomes sharper, while the others are attenuated. We should remark that a quite similar result has been obtained for the quark spectral density in a QGP [16,18], where the quarks are coupled with massive scalar or vector-bosonic modes in the plasma.

In order to elucidate the physical meanings of the observed peaks at intermediate temperature $T/v_0 = 0.5$, we compare in Fig. 5 the peak positions of $\rho_+^{(\nu)}$ seen in the middle panel of Fig. 4 with the massless-HTL [12] dispersion relation $\omega_{\mathrm{HTL}}(|\mathbf{p}|)$, which is defined as a solution of

$$\omega_{\mathrm{HTL}} - |\mathbf{p}| - \mathrm{Re}\Sigma_{+,\mathrm{HTL}}^{(\nu)}(|\mathbf{p}|, \omega_{\mathrm{HTL}}; T) = 0. \quad (36)$$

Here, the real part of the self-energy $\mathrm{Re}\Sigma_{+,\mathrm{HTL}}^{(\nu)}$ is given by taking the limit $T \gg \omega, |\mathbf{p}|, M_{\mathrm{W,Z}}$ in the full one-loop result, as detailed in Appendix D. Figure 5 shows that the positive (negative) branch in $\rho_+^{(\nu)}$ corresponds to the quasiparticle (antiplasmino) mode, which is the familiar solution appearing in the massless-HTL approximation.

Although Eq. (36) has a solution in the ultrasoft region $\omega_{\mathrm{HTL}}(|\mathbf{p}|) \sim 0$ with $|\mathbf{p}|$ being finite, the imaginary part in the massless-HTL approximation $\mathrm{Im}\Sigma_{\pm,\mathrm{HTL}}$ becomes huge, and kills the peak structure at the ultrasoft region $\omega_{\mathrm{HTL}}(|\mathbf{p}|) \sim 0$. Thus, the emergence of the collective modes near the origin (ultrasoft mode) is characteristic of the full spectral density $\rho_+^{(\nu)}$.

In the higher-temperature region $T \gg M_{\mathrm{W,Z}}$, the two peaks in the positive- and negative-energy regions become sharper while the central peak is greatly attenuated [see the right panel in Fig. 4 ($T/v_0 = 0.8$)]. As shown in Fig. 6, these two peaks approximately stay at the same position as the quasiparticle (antiplasmino) mode of the massless-HTL approximation. Thus, the general property of the spectral density becomes closer to that of the massless-HTL approximation in the high-temperature region $T \gg M_{\mathrm{W,Z}}$. We note that the high-temperature region does not satisfy the condition $T \ll v(T)$; therefore, higher-loop corrections may be non-negligible. In fact, it is known that a resummation of higher-loop diagrams is necessary for the ultrasoft-momentum region ω, $|\mathbf{p}| \lesssim g^2 T$ in QED and QCD [32], where a resummation scheme is developed for obtaining sensible results. It would be interesting to develop such a resummation scheme in the electroweak theory and investigate the spectral properties in the vicinity of the electroweak

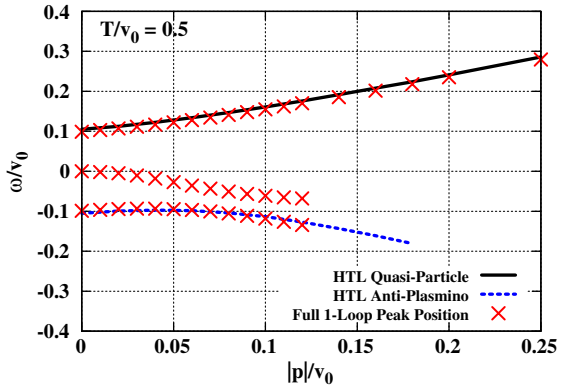

FIG. 5 (color online). The comparison between the peak position of the spectral density $\rho_+^{(\nu)}$ shown in the middle panel of Fig. 4 and the HTL dispersions given by Eq. (36) at $T/v_0 = 0.5$ in the ω-$|\mathbf{p}|$ plane.

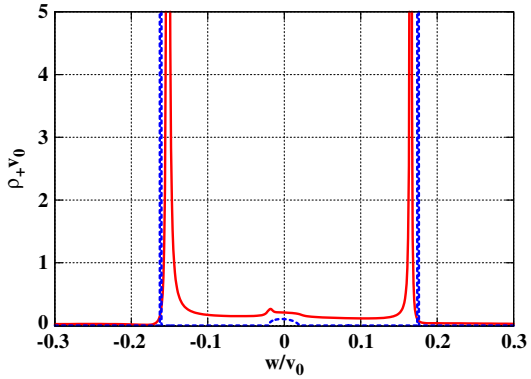

FIG. 6 (color online). The spectral density $\rho_+^{(\nu)}$ (solid red line) as a function of ω at $(|\mathbf{p}|/v_0, T/v_0) = (0.02, 0.8)$ compared with the spectral density obtained by using the massless-HTL approximation (dashed blue line) for the same conditions.

phase transition, which is, however, beyond the scope of the present work and left as a future task.

B. Emergence of the three-peak structure

In this subsection, we investigate the properties of the three-peak structure in detail.

In the upper panels of Fig. 7, we show the imaginary part of the self-energy, $\mathrm{Im}\Sigma_{\pm}^{(\nu)}$, given by Eq. (C10) as a function of ω/v_0 at $(|\mathbf{p}|/v_0, T/v_0) = (0.02, 0.5)$. Because of the growing statistical factors [Eqs. (B10) and (B11)] with increasing temperature, the Landau damping effect becomes significant, and the imaginary part of the self-energy $\mathrm{Im}\Sigma_{+}^{(\nu)}$ drastically grows in the space-like region. A remarkable point is that $\mathrm{Im}\Sigma_{+}^{(\nu)}$ stays relatively small in the vicinity of $\omega \sim 0$, and has two peaks in the space-like region ($\omega^2 \leq |\mathbf{p}|^2$). By utilizing the Kramers-Kronig-like dispersion relation (C7) (which we call the Kramers-Kronig relation to avoid confusion with the dispersion relation as the momentum dependence of energy), the real part inevitably shows an oscillatory behavior, as displayed in the middle panel of Fig. 7. The crossing points with the straight dashed line representing $y = \omega - |\mathbf{p}|$ correspond to the solutions of the equation

$$\mathcal{D}_{+}^{(\nu)}(|\mathbf{p}|, \omega; T, \xi) = 0. \tag{37}$$

Here, $\mathcal{D}_{+}^{(\nu)}$ is defined in Eq. (35). Two of the solutions lead to the two peaks of the imaginary part, and hence do not lead to a peak in the spectral density. The remaining three solutions contribute to the peaks in the spectral density (lower panel of Fig. 7). We note that in the previous QGP studies [16,18] similar results for the real and imaginary parts of the self-energy have been obtained, and the mechanism of the emergence of the three peaks in the spectral density was interpreted in terms of a resonant scattering [16].

In order to have a more complete overview, we show the solution of Eq. (37) in the full ω-$|\mathbf{p}|$ plane for $T/v_0 = 0.35$, 0.42, and 0.5 cases in Fig. 8; the resultant function $\omega(|\mathbf{p}|)$ is called the quasidispersion relation. The upper panel ($T/v_0 = 0.35$) corresponds to the dispersion relation at a characteristic temperature satisfying $T/M_{\mathrm{W,Z}} \sim 1$, where the Landau damping effects start to dominate. The quasidispersion curve deviates from the light cone, and shows a rapid increase for $0.03 \leq |\mathbf{p}|/v_0 \leq 0.04$. As T is increased, this steep-rise behavior is evolved to a "backbending" shape as shown in the middle panel of Fig. 8 ($T/v_0 = 0.42$). Eventually, the branch with the backbending part crosses the ω axis around $T/v_0 \simeq 0.475$, at which point the additional two branches appear in the negative-ω region; see the lower panel of Fig. 8. Thus, we get five branches in the low-momentum region. At $|\mathbf{p}|/v_0 = 0.02$, these branches correspond to the five crossing points in the middle panel of Fig. 7.

We should mention that a similar branch of the neutrino dispersion relation was found in the HTL approximation

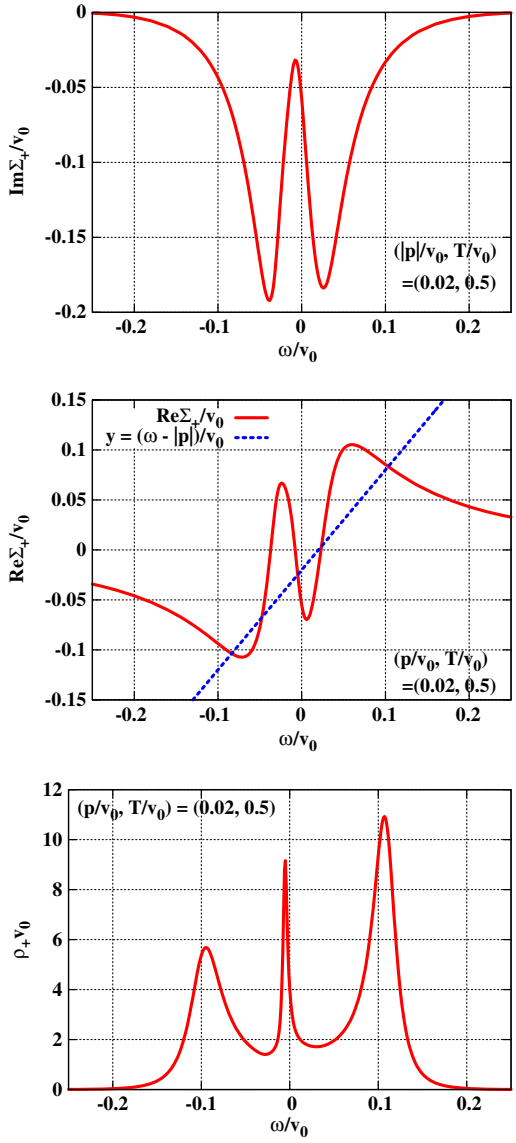

FIG. 7 (color online). The self-energies $\mathrm{Im}\Sigma_{+}^{(\nu)}/v_0$ (upper), $\mathrm{Re}\Sigma_{+}^{(\nu)}/v_0$ (middle), and the spectral density $\rho_{+}^{(\nu)}v_0$ at $(|\mathbf{p}|/v_0, T/v_0) = (0.02, 0.5)$.

with the unitary gauge in Ref. [15], and the branch that touches the ω axis is called a *pitchfork bifurcation*. In Ref. [15], the pitchfork bifurcation is found to start when the T-dependent mass scale $\Delta = 2M_{\mathrm{W}}^2(T)/(gT^2)$ exceeds $\Delta_c \simeq 1.275$. In the present study, the pitchfork bifurcation starts from $T/v_0 \simeq 0.475$, corresponding to $\Delta_c \simeq 1.28$, which is consistent with the finding in the previous work [15], and suggests the gauge independence of the temperature at which the bifurcation starts.

C. Gauge parameter ξ dependence of the three-peak structure

So far, we have investigated the spectral density $\rho_{+}^{(\nu)}$ in the 't Hooft-Feynman gauge ($\xi = 1$), and found the three-peak structure that consists of the ultrasoft mode as

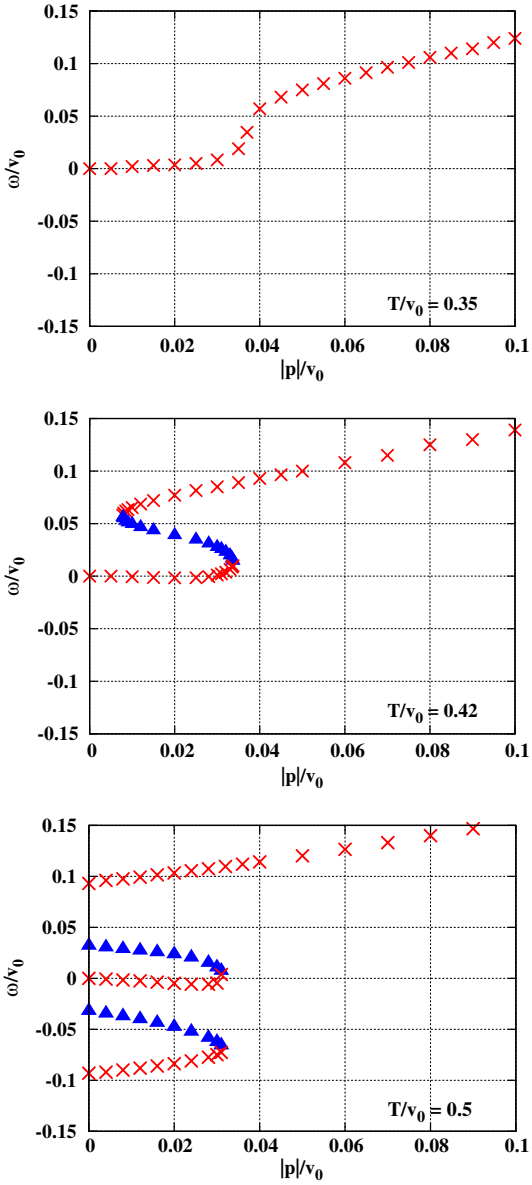

FIG. 8 (color online). The dispersion relations at $T/v_0 = 0.35$ (upper), 0.42 (middle), and 0.5 (lower). The cross symbol corresponds to a solution of Eq. (37) that gives a peak to the spectral density. The triangle symbol is a solution of Eq. (37) with a large imaginary part.

well as the quasiparticle and antiplasmino modes. In this subsection, we investigate the ξ (in)dependence of the three-peak structure.

In Fig. 9, we show the neutrino self-energies for the gauge parameter $\xi = 0.1,\ 1,\ 10$. We also display the unitary-gauge result which has been obtained by utilizing the Proca formalism [16], which corresponds to $\xi \to \infty$. The momentum and temperature are set to be the same as in Fig. 7, $(|\mathbf{p}|/v_0, T/v_0) = (0.02, 0.5)$. As shown in the figure, the ξ dependence becomes significant with increasing ω. However, in the low-energy region $\omega/v_0 \lesssim 0.15$, where the three-peak structure emerges in the neutrino spectral density, the ξ dependence is found to be negligible in both the imaginary part (upper panel) and the real part (lower panel). This indicates that both the position and the width of the three peaks are independent of the gauge parameter ξ.

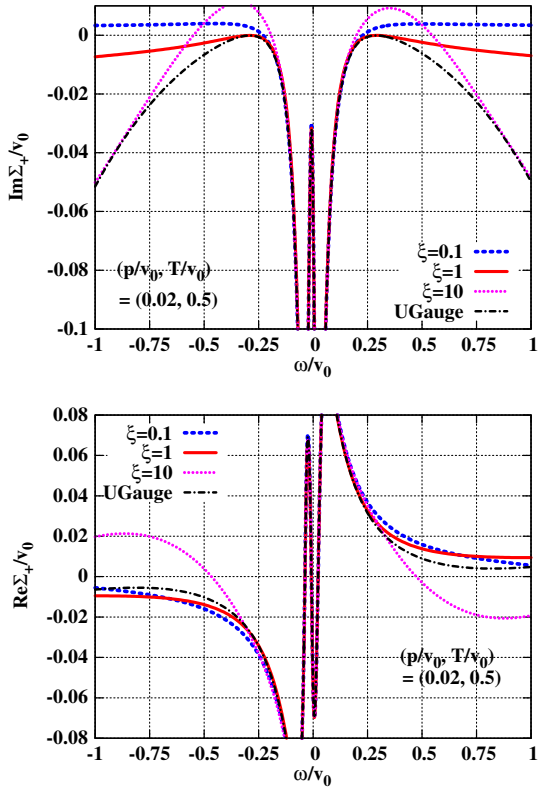

FIG. 9 (color online). The gauge parameter (ξ) dependence of the imaginary (upper) and real (lower) parts of neutrino self-energies at $(|\mathbf{p}|/v_0, T/v_0) = (0.02, 0.5)$. As shown in Fig. 7, the three-peak structure appears in the low-energy region, $|\omega/v_0| \lesssim 0.15$, where the ξ dependence is negligible.

For the three peaks of the spectral density, the two conditions $M_{W,Z} \gg \omega, |\mathbf{p}|$ and $T \gg \omega, |\mathbf{p}|$ are satisfied. Because of the former condition, the unitary-gauge part of the self-energy dominates [see Eqs. (C2) and (C3)], which accounts for the ξ independence of the three-peak structure. By using both conditions, we can define an extension of the HTL approximation to the case where the boson mass is finite—which we call the *massive-HTL* expansion—for the neutrino self-energy, as detailed in Appendix E. The leading-order terms reproduce the self-energy derived in Ref. [15]. The temperature and energy region for the pitchfork bifurcation explained in the previous subsection is in the validity region of this approximation scheme, which accounts for the gauge invariance of Δ_c and the agreement of its values in the present and the previous study [15].

IV. NEUTRINO SPECTRAL DENSITY AT $T \geq T_c$

In the previous sections, we have investigated the neutrino spectral properties in the broken phase. In this section, we discuss their properties in the symmetric phase $T \geq T_c$.

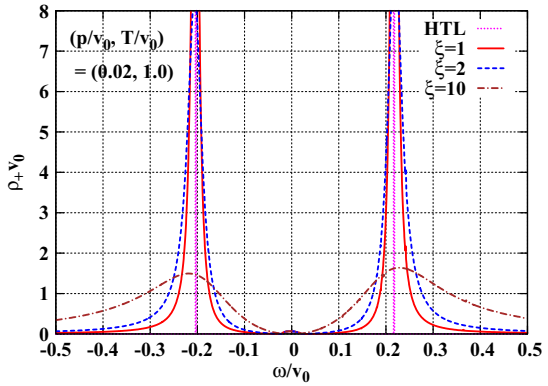

FIG. 10 (color online). The gauge parameter (ξ) dependence of the neutrino spectral density at $|\mathbf{p}|/v_0 = 0.02$ in the symmetric phase $T/v_0 = 1.0 > T_c$.

In the symmetric phase, the weak bosons become massless, as is clear from Eq. (12). Although higher-loop corrections for the weak-boson masses as well as the neutrino self-energy may become non-negligible in the symmetric phase, in particular, for $\omega, |\mathbf{p}| \ll g^2 T$, we dare to analyze the neutrino self-energy within the present approximation and show an advantageous property of R_ξ gauge: in the unitary gauge, the massless limit $M \to 0$ leads to the divergence in the self-energy due to the prefactor proportional to $1/M^2$ in the imaginary part [Eq. (C2)], and hence the massless limit cannot be well defined within the unitary gauge. This problem is solved in R_ξ gauge by the additional ξ-dependent part [Eq. (C3)]: all $\mathcal{O}(M^{-2})$ terms beautifully cancel out between the unitary-gauge part [Eq. (C2)] and the ξ-dependent part [Eq. (C3)], and we find the finite imaginary part of the self-energy in the vanishing gauge-boson masses ($T, \omega, |\mathbf{p}| \gg M \to 0$) as

$$\begin{aligned}
&\mathrm{Im}\sigma_\pm(|\mathbf{p}|, \omega; T)|_{\mathrm{M}\to 0} \\
&= \frac{\pm 1}{32\pi|\mathbf{p}|^2}[-(1-\xi)|\mathbf{p}|p^2[N_{\mathrm{F}}(X_\mp) \\
&\quad + N_{\mathrm{B}}(Y_\mp)] + [(1-\xi)(\omega \pm |\mathbf{p}|)^2 + 2p^2] \\
&\quad \cdot T I_{\mathrm{ST}}(X_+, X_-; \omega/T) - 4(\omega \mp |\mathbf{p}|) \\
&\quad \cdot T^2 J_{\mathrm{ST}}(X_+, X_-; \omega/T)], \qquad (38)
\end{aligned}$$

where I_{ST} and J_{ST} have been defined in Eqs. (B10) and (B11), and their arguments $X_\pm$, $Y_\pm$ are defined by

$$(X_\pm, Y_\pm) \equiv \left(\frac{\omega \mp |\mathbf{p}|}{2T}, \frac{-\omega \mp |\mathbf{p}|}{2T}\right). \qquad (39)$$

The technical details to derive Eq. (38) are provided in Appendix F.

Furthermore, the cancellations of $\mathcal{O}(M^{-2})$ terms are also found in the imaginary part of the vacuum self-energy [$\mathrm{Im}\sigma_{\pm,0} \equiv$ Eqs. (C4) + (C5)], which reads

$$\mathrm{Im}\sigma_{\pm,0}(|\mathbf{p}|, \omega)|_{\mathrm{M}\to 0} = \frac{-\mathrm{sgn}(\omega)\xi}{16\pi}\theta(p^2)(\omega \mp |\mathbf{p}|). \qquad (40)$$

In Fig. 10, we show the neutrino spectral density at $|\mathbf{p}|/v_0 = 0.02$ in the symmetric phase $T/v_0 = 1.0 > T_c$ for $\xi = 1, 2, 10$. We find the quasiparticle and the anti-plasmino peaks, whose positions are almost independent of ξ and consistent with the HTL results [11]. One sees that the width seems to have a significant ξ dependence. It should be noted, however, that it was shown in Ref. [18] that at one-loop order the condition $\xi \lesssim 1/g$ guarantees the smallness of the gauge dependence. Since $g \simeq 0.7$, the upper limit of ξ seems to be $\simeq 1.4$. This estimate shows that the gauge dependence seen in Fig. 10 is consistent with the analysis in Ref. [18] and tells us that we should restrict ourselves to $\xi \lesssim 2$ to get a sensible result.

V. DISCUSSION: TOWARD APPLICATION TO RESONANT LEPTOGENESIS

There is a growing interest in the collective nature of the fermion quasiparticles in the scenario of thermal leptogenesis [33–40] because the novel collective fermion modes may significantly modify lepton number creation. In this section, we argue that the neutrino collective modes with the three peaks in the spectral function obtained in the previous sections could possibly affect leptogenesis and hence the BAU.

In thermal leptogenesis, the Lagrangian is extended to include the right-handed neutrinos (N_{R}^i, $i = 1, 2, 3$),

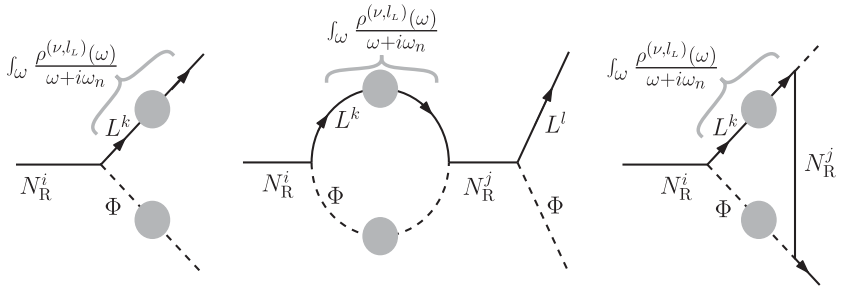

FIG. 11. The diagram of the N_{R}^i decay to a left-handed lepton $L^i = (\nu^i, l_{\mathrm{L}}^i)^T$ and a Higgs doublet Φ. Note that the lepton propagators in all the diagrams are given in terms of the spectral densities $\rho^{(\nu)}$ and $\rho^{(l_{\mathrm{L}})}$.

$$\delta\mathcal{L} = \bar{N}^i_{\rm R} i\not{\partial} N^i_{\rm R} + Y_{ij}\bar{N}^i_{\rm R}\Phi^\dagger L^j - \frac{M^{ij}_{\rm R}}{2}\bar{N}^i_{\rm R}N^j_{\rm R} + \text{H.c.}, \quad (41)$$

where L^i and Φ represent the standard model left-handed lepton $(\nu^i, l^i_{\rm L})^T$ and the standard model Higgs doublet, respectively. The Yukawa interaction (Y_{ij}) term in Eq. (41) gives rise to the $N_{\rm R}$ decay shown in Fig. 11, which causes lepton number creation. The leading effects on the finite-T interaction rate are given by the left diagram in Fig. 11, and are expressed as

$$\Gamma^i_{\rm N}(p) = -\frac{1}{2p_0}\,\mathrm{tr}_{\rm spin}[(\not{p} + M^i_{\rm R})\mathrm{Im}\Sigma_{\rm N}(p)], \quad (42)$$

$$\Sigma_{\rm N}(p) = -4(Y^\dagger Y)_{11} T\sum_n \int \frac{d^3k}{(2\pi)^3}\tilde{G}_{\rm F}(k)\tilde{G}_{\rm S}(p-k), \quad (43)$$

where we have adopted the mass basis $M^{ij}_{\rm R} = \delta^{ij}M^i_{\rm R}$, and $\tilde{G}_{\rm F}$ and $\tilde{G}_{\rm S}$ represent the full finite-T propagators of a lepton and the Higgs particle, respectively. The $\tilde{G}_{\rm F}$ is expressed in terms of the spectral density $\rho^{(\nu,l_{\rm L})}(\mathbf{k}, \omega; T)$ of the left-handed neutrino ν (or the charged lepton $l_{\rm L}$) as follows:

$$\tilde{G}_{\rm F}(\mathbf{k}, i\omega_n; T) = \int_{-\infty}^{\infty} d\omega \frac{\rho^{(\nu,l_{\rm L})}(\mathbf{k}, \omega; T)}{\omega + i\omega_n}. \quad (44)$$

At the electroweak scale, the spectral density $\rho^{(\nu)}$ in Eq. (44) can have the three-peak structure, as was shown in the previous section. Then—assuming resonant leptogenesis at this scale [4]—these collective modes corresponding to the peaks would modify the creation rate of the lepton number $\Gamma^i_{\rm N}$. Moreover, the spectral density having the three peaks is involved in both the leading and subleading diagrams shown in Fig. 11, and modifies their interference effects leading to the CP asymmetry.

Here a natural question is whether the $N_{\rm R}$ decay into ν with the collective nature which leads to leptogenesis can take place before the sphaleron freeze-out. If not, the three-peak structure would not have any relation to the BAU. In order to study this problem, we shall estimate the sphaleron freeze-out temperature T_*, and investigate the spectral density of ν in the vicinity of T_*.

The net baryon number $N_{\rm b}$ is produced in the sphaleron process when the changing rate of $N_{\rm b}$ is larger than the expanding rate of the universe $H(T)$,

$$\left|\frac{1}{N_{\rm b}}\frac{dN_{\rm b}}{dt}\right| \geq H(T). \quad (45)$$

The freeze-out temperature T_* is obtained from the equality in Eq. (45). The expanding rate $H(T)$ is given by the Hubble parameter in the early universe at temperature T,

$$H(T) = 1.66\sqrt{N_{\rm dof}}\frac{T^2}{M_{\rm PL}} \simeq T^2 \times 1.41 \times 10^{-18}\ (\text{GeV}), \quad (46)$$

with radiation degrees of freedom for the SM $N_{\rm dof} \simeq 106.75$, and the Planck mass $M_{\rm PL} \simeq 1.22 \times 10^{19}$ (GeV).

We evaluate the changing rate of the net baryon number [2],

$$\frac{1}{N_{\rm b}}\frac{dN_{\rm b}}{dt} = -1100\ \mathrm{K}(\lambda/g^2)g^7 v(T) \times \exp\left[-\frac{E_{\rm sph}(g, \lambda, v(T))}{T}\right], \quad (47)$$

by using the same electroweak parameter set and Higgs potential as those used in the study of the neutrino spectral density (see Table I). Under the static sphaleron background, its free energy is known to have the expression

$$E_{\rm sph} = \frac{4\pi v(T)}{g}F_0(\lambda/g^2), \quad (48)$$

where the dimensionless function $F_0(\lambda/g^2)$ is estimated to be

$$F_0(\lambda/g^2) = F_0(m^2_{\rm H}/(2g^2v_0^2)) \simeq F_0(0.309) \simeq 1.89. \quad (49)$$

In the second relation we have used the values listed in Table I for $m_{\rm H}$, v_0, g. In the final relation, we have taken the results $F_0(0.1) = 1.83$ and $F_0(1.0) = 2.10$ from Table II in Ref. [8], and performed a linear interpolation to estimate $F_0(0.309)$.

The function $K(\lambda/g^2)$ is responsible for quantum fluctuations around the sphaleron vacuum, and is well approximated by using the expression [41]

$$K\left(\frac{\lambda}{g^2}\right) = \exp\left[-0.09\left(\frac{\lambda}{g^2} - 0.4\right)^2 - 0.13\left(\frac{g^2}{\lambda} - 2.5\right)^2\right] \simeq 0.93, \quad (50)$$

where again we have used the values listed in Table I.

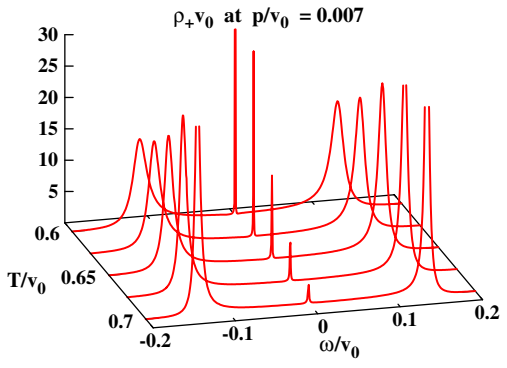

FIG. 12 (color online). The neutrino spectral density $\rho^{(\nu)}_+ v_0$ in the vicinity of a sphaleron freeze-out temperature $T_*/v_0 \sim 0.65$ at a fixed low momentum $p/v_0 = 0.007$.

Substituting Eqs. (48)–(50) into Eq. (47), the changing rate of the net baryon number is obtained as

$$\left|\frac{1}{N_{\rm b}}\frac{dN_{\rm b}}{dt}\right| \simeq 51.02 v(T) \exp\left[-36.51\frac{v(T)}{T}\right]. \quad (51)$$

By using Eqs. (46) and (51) as well as Eq. (16), the inequality (45) reduces to the following condition:

$$T \geq T_* \simeq 160 \text{ GeV}. \quad (52)$$

The leptons created at a temperature satisfying $T/v_0 \geq T_*/v_0 \sim 0.65$ can contribute to the BAU via the sphaleron process. Figure 12 shows the neutrino spectral density $\rho_+^{(\nu)} v_0$ for various temperatures around T_* at a fixed low momentum $p/v_0 = 0.007$, for which the sharp peaks are observed in the ultrasoft region $\omega \sim 0$. Thus, the three-peak structure is still observed in this temperature region for small momenta, although the strength of the ultrasoft mode may not be so strong. This indicates that the three-peak collective modes of ν could affect leptogenesis before the freeze-out. It is interesting that such a possibility is shown in the definite setup. We note that the condition $T/v_0 \sim 0.65$ corresponds to $T \sim v(T)$; see Fig. 2. As explained in Sec. II B, higher-loop corrections start to be non-negligible around this temperature, and should be taken into account to get more sensible results. We leave this task as a future work.

VI. SUMMARY AND CONCLUDING REMARKS

We have investigated the spectral properties of standard model left-handed neutrinos without restricting ourselves to the HTL approximation, in the full energy-momentum plane at finite T around the electroweak scale. This analysis is motivated by the scenario of electroweak-scale resonant leptogenesis [3,4], where the spectral property of left-handed neutrinos can affect lepton number creation through the decay process of right-handed neutrinos $N_{\rm R}$, as shown in Fig. 1. We have employed the R_ξ gauge in order to investigate the possible gauge-fixing dependence of the spectral density.

In the intermediate-temperature region $M_{\rm W,Z} \lesssim T$ ($M_{\rm W,Z}$ is the weak-boson mass at finite T), the neutrino spectral density involves an ultrasoft mode as well as normal and antiplasmino modes, and shows a three-peak structure. The three-peak structure emerges independently of the gauge parameter, although a detailed structure of the spectral density may have a slight gauge dependence. Its emergence is accompanied by a pitchfork bifurcation of the neutrino dispersion relation, consistent with the previous finding in Ref. [15], where the HTL approximation was adopted solely in the unitary gauge. We have mentioned that the mechanism of the emergence of the collective excitations and the three-peak structure is similar to what was discussed in Ref. [16] in a different context.

We have examined the neutrino spectral densities in the symmetric phase by taking the limit of vanishing gauge-boson masses ($M_{\rm W,Z} \to 0$). In this limit, the self-energy in the unitary gauge shows a divergence, which completely cancels out in the R_ξ gauge. Thus, the R_ξ gauge fixing has allowed us to investigate the symmetric phase. The neutrino spectral properties in the symmetric phase are found to be similar to that in the HTL approximation. We have found that the possible gauge dependence of the width of the peaks in the spectral function is controllable, and the gauge parameter ξ should be restricted to $\xi \lesssim 2$ to have a sensible result.

We have also discussed a possible implication of the present study for particle cosmology, in particular in the resonant leptogenesis scenario, where it makes sense to consider a thermal leptogenesis at electroweak scale temperature. We have pointed out that the collective modes of left-handed neutrinos provide a novel decay channel in the decay processes of the right-handed neutrinos, and could modify lepton number creation. We have estimated the sphaleron freeze-out temperature T_* and investigated the spectral density in the vicinity of T_*. Within the present setup with the second-order electroweak phase transition, the ultrasoft as well as (anti) plasmino modes can appear at a temperature comparable to T_*, though the strength of ultrasoft modes might not be so strong. Thus, the novel three-peak collective modes could affect leptogenesis at $T \gtrsim T_*$, and, therefore, baryogenesis.

There are several subjects to be studied in the future. First, it is desirable to estimate how large the effects of two-loop or higher-order diagrams are on the neutrino spectral density. Second, the present formulation should be extended to include the bare-fermion-mass effects [17]. Finally, it would be interesting to evaluate lepton number creation with respect to the nontrivial spectral properties of the neutrinos as well as the charged leptons by adopting the explicit model of resonant leptogenesis.

ACKNOWLEDGMENTS

We thank Chee Sheng Fong for fruitful discussions on resonant leptogenesis. We thank Marco Drewes for useful comments on the quantum effects in the thermal leptogenesis and information on some references. This work was supported by JSPS KAKENHI Grants No. 20540265, No. 23340067, No. 2456384, and No. 24740184. T. K. was partially supported by the Yukawa International Program for Quark-Hadron Sciences, and by a Grant-in-Aid for the global COE program "The Next Generation of Physics, Spun from Universality and Emergence" from MEXT. D. S. was supported by JSPS Strategic Young Researcher Overseas Visits Program for Accelerating Brain Circulation (No. R2411).

TABLE I. The parameters of electroweak theory. The entries in the third column are the values used in this paper. The $SU_W(2)$ gauge coupling g is chosen to reproduce approximate experimental values of W- and Z-boson masses at $T = 0$.

Parameters	Symbols	Values in this work
Higgs VEV at $T = 0$	v_0	246 GeV
Higgs mass at $T = 0$	m_H	126 GeV
Weinberg angle	θ_w	$\sin^2\theta_w = 0.2325$
$SU_W(2)$ gauge coupling	g	0.6515
$U_Y(1)$ gauge coupling	$g' = g\tan\theta_w$	~0.3586
$U_{EM}(1)$ gauge coupling	$e = g\sin\theta_w$	~0.3141
W-boson mass	$m_W = v_0 g/2$	~80 GeV
Z-boson mass	$m_Z = m_W/\cos\theta_w$	~91 GeV

APPENDIX A: PARAMETERS OF ELECTROWEAK THEORY

We summarize the parameters of electroweak theory and their values that were used in this paper in Table I.

APPENDIX B: LANDAU DAMPING WITH MASSIVE GAUGE BOSON

In this appendix, we briefly review so-called Landau damping, a scattering of a probe fermion by thermally excited particles. We closely follow Ref. [16].

The effects of the thermal background on the probe particle are involved in the one-loop retarded self-energy $\sigma^{\rm ret}$ given by Eqs. (24)–(26). Taking the imaginary part of these equations, we obtain

$$\begin{aligned}&\mathrm{Im}\sigma_U^{\rm ret}(\mathbf{p},\omega;T,M)\\&= -\pi\sum_{s,t=\pm}\int\frac{d^3k}{(2\pi)^3}\frac{t\gamma^\mu\Lambda_{s,\mathbf{k}}\gamma^0\gamma^\nu}{2E_{\mathbf{q}}}\left(g_{\mu\nu}-\frac{q_\mu q_\nu}{M^2(T)}\right)\\&\quad\times[N_F(s|\mathbf{k}|/T)+N_B(-tE_{\mathbf{q}}/T)]\delta_{\omega-s|\mathbf{k}|-tE_{\mathbf{q}}},\end{aligned}\tag{B1}$$

$$\begin{aligned}&\mathrm{Im}\sigma_\xi^{\rm ret}(\mathbf{p},\omega;T,M)\\&= -\pi\sum_{s,t=\pm}\int\frac{d^3k}{(2\pi)^3}\frac{t\gamma^\mu\Lambda_{s,\mathbf{k}}\gamma^0\gamma^\nu}{2E_{\mathbf{q}}^\xi(M)}\frac{q_\mu q_\nu}{M^2(T)}\\&\quad\times[N_F(s|\mathbf{k}|/T)+N_B(-tE_{\mathbf{q}}^\xi/T)]\delta_{\omega-s|\mathbf{k}|-tE_{\mathbf{q}}^\xi},\end{aligned}\tag{B2}$$

where N_F (N_B) represents the Fermi-Dirac (Bose-Einstein) distribution functions [see Eq. (27)]. The delta functions provide the momentum-conservation conditions in the presence of massive gauge-boson effects,

$$E_{\mathbf{q}=\mathbf{p}-\mathbf{k}}(M) = \sqrt{|\mathbf{q}|^2+M^2(T)},\tag{B3}$$

$$E_{\mathbf{q}}^\xi(M) \equiv E_{\mathbf{q}}(\sqrt{\xi}M).\tag{B4}$$

Here, $M(T)$ represents the W-boson, Z-boson, or photon mass at finite T.

The physical meaning of the delta functions and distribution functions in Eqs. (B1) and (B2) is more transparent when they are rewritten as

$$\begin{aligned}&st=++:\delta_{\omega-|\mathbf{k}|-E_{\mathbf{q}}}[(1-N_F)(1+N_B)+N_FN_B],\\&st=-+:\delta_{\omega+|\mathbf{k}|-E_{\mathbf{q}}}[N_F(1+N_B)+N_B(1-N_F)],\\&st=+-:\delta_{\omega-|\mathbf{k}|+E_{\mathbf{q}}}[N_B(1-N_F)+N_F(1+N_B)],\\&st=--:\delta_{\omega+|\mathbf{k}|+E_{\mathbf{q}}}[N_FN_B+(1-N_F)(1+N_B)],\end{aligned}\tag{B5}$$

where $N_F = N_F(+|\mathbf{k}|/T)$ and $N_B = N_B(+E_{\mathbf{q}}/T)$ or $N_B(+E_{\mathbf{q}}^\xi/T)$. These terms can be interpreted in terms of a scattering process of the probe fermion with the thermal background. A thermally excited fermion has a statistical factor N_F in the initial state and $(1-N_F)$ in the final state due to Pauli blocking. Similarly, a thermally excited boson has a factor N_B in the initial state and $(1+N_B)$ in the final state representing the induced emission. These thermal particles are all on-shell in the present approximation. We note that the second and third lines in Eq. (B5) involve the thermal particles as incident particles. Then the first term in the second line of Eq. (B5) is interpreted as a scattering process of an external lepton with a thermally excited lepton carrying a factor N_F into a thermally excited gauge boson carrying a factor $1+N_B$. The second term is its inverse process. The third line in Eq. (B5) describes processes with the incident and the final states exchanged in the second line. These processes are known as Landau damping, and make decay channels in the space-like region. The same interpretation holds for the ξ-dependent part with a replacement $E_{\mathbf{q}} \to E_{\mathbf{q}}^\xi$. The Landau damping, which is absent at vanishing temperature, becomes significant at high temperature where thermally excited particles are abundant.

For the space like–region terms ($st = -+$ and $+-$), the momentum integral in the unitary-gauge part of Eq. (B1) is evaluated as

$$\begin{aligned}&\sum_{st=-+,+-}st\int\frac{d^3k}{(2\pi)^3}\delta_{\omega-s|\mathbf{k}|-tE_{\mathbf{q}}}\\&=\sum_{st=-+,+-}\frac{st}{4\pi^2}\int_0^\infty d|\mathbf{k}||\mathbf{k}|^2\int_{-1}^1 d(\cos\eta)\delta_{\omega-s|\mathbf{k}|-tE_{\mathbf{q}}}\\&=\frac{-T^3}{4\pi^2}\left[\int_{-\infty}^{x_+}+\int_{x_-}^{\infty}\right]dx=\frac{T^3}{4\pi^2}\left[\int_{x_+}^{x_-}-\int_{-\infty}^{\infty}\right]dx,\end{aligned}\tag{B6}$$

where

$$x_\pm = \frac{p^2-M^2}{2T(\omega\pm|\mathbf{p}|)},\tag{B7}$$

and $\cos\eta$ denotes the angle between external and internal fermion momenta $\mathbf{p}$ and $\mathbf{k}$. Repeating the same procedure in the time-like region, only the contribution from the $\int_{x_+}^{x_-}$ term remains.

Substituting Eq. (B6) into Eq. (B1), the combination of the integrals $\int_{-\infty}^{\infty}$ and/or $\int_{x_+}^{x_-}$ with the statistical factors $N_F(s|\mathbf{k}|/T) + N_B(-tE_\mathbf{q}/T)$ gives rise to two types of integrals,

$$I_{ST}(x_+, x_-; \omega/T) \equiv \left[\int_{x_+}^{x_-} - \theta(-p^2)\int_{-\infty}^{\infty}\right] dx[N_F(x) + N_B(x - \omega/T)], \tag{B8}$$

$$J_{ST}(x_+, x_-; \omega/T) \equiv \left[\int_{x_+}^{x_-} - \theta(-p^2)\int_{-\infty}^{\infty}\right] dx x[N_F(x) + N_B(x - \omega/T)]. \tag{B9}$$

Here, the step function $\theta(-p^2)$ with $p^2 = \omega^2 - |\mathbf{p}|^2$ picks up the space-like region. The integral $\int_{-\infty}^{\infty}$ is analytically performed, and reads

$$I_{ST}(x_+, x_-; \omega/T) = \left[\int_{x_+}^{x_-} dx N_F(x) + \int_{y_+}^{y_-} dy N_B(y)\right] + \theta(-p^2)\frac{\omega}{T}, \tag{B10}$$

$$J_{ST}(x_+, x_-; \omega/T) = \left[\int_{x_+}^{x_-} dx x N_F(x) + \int_{y_+}^{y_-} dy y N_B(y)\right] + \frac{\omega}{T}\int_{y_+}^{y_-} dy N_B(y) - \theta(-p^2) \times \left[\frac{\pi^2}{2} - \frac{\omega^2}{2T^2}\right], \tag{B11}$$

where

$$y_\pm = x_\pm - \omega/T. \tag{B12}$$

The remaining integrals $\int_{x_+}^{x_-}$ and $\int_{y_+}^{y_-}$ will be numerically evaluated. For the ξ-dependent part, the counterparts of I_{ST} and J_{ST} are obtained by the replacements

$$x_\pm \to x'_\pm = \frac{p^2 - \xi M^2}{2T(\omega \pm |\mathbf{p}|)}, \tag{B13}$$

$$y_\pm \to y'_\pm = x'_\pm - \frac{\omega}{T}. \tag{B14}$$

As will be shown in the next appendix, I_{ST} and J_{ST} give a key ingredient to the imaginary part of the self-energy [see Eqs. (C2) and (C3)].

APPENDIX C: SELF-ENERGY $\sigma_\pm$ AT FINITE T

Based on previous work [16,18], we review the derivation of the self-energy $\sigma_\pm$ defined in Eq. (29). We start from calculating the imaginary part of $\sigma_\pm$, which is composed of the unitary-gauge part and the ξ-dependent part,

$$\mathrm{Im}\sigma_\pm(|\mathbf{p}|, \omega; T, M) = \mathrm{Im}\sigma^U_\pm(|\mathbf{p}|, \omega; T, M) + \mathrm{Im}\sigma^\xi_\pm(|\mathbf{p}|, \omega; T, M). \tag{C1}$$

Substituting the imaginary part of the retarded self-energy [Eqs. (B1) and (B2)] into Eq. (29), the straightforward computations lead to

$$\mathrm{Im}\sigma^U_\pm(|\mathbf{p}|, \omega; T, M) = \frac{\pm 1}{32\pi|\mathbf{p}|^2M^2}[(-p^2 + M^2)((\omega \mp |\mathbf{p}|)^2 - 2M^2) \cdot T I_{ST}(x_+, x_-; \omega/T) + 2(\omega \mp |\mathbf{p}|)(p^2 - 2M^2) \cdot T^2 J_{ST}(x_+, x_-; \omega/T)], \tag{C2}$$

and

$$\mathrm{Im}\sigma^\xi_\pm(|\mathbf{p}|, \omega; T, M) = \frac{\pm 1}{32\pi|\mathbf{p}|^2M^2}[(p^2 - \xi M^2)(\omega \mp |\mathbf{p}|)^2 \cdot T I_{ST}(x'_+, x'_-; \omega/T) - 2p^2(\omega \mp |\mathbf{p}|) \cdot T^2 J_{ST}(x'_+, x'_-; \omega/T)]. \tag{C3}$$

The integrals I_{ST} and J_{ST} are given by Eqs. (B10) and (B11), respectively. In the zero-temperature limit, keeping the relations $T < M$, ω, $|\mathbf{p}|$, we obtain the *vacuum* effects

$$\mathrm{Im}\sigma^U_{\pm,0}(|\mathbf{p}|, \omega; M) \equiv \mathrm{Im}\sigma^U_\pm(|\mathbf{p}|, \omega; M, T \to 0) = \frac{-\mathrm{sgn}(\omega)(\omega \mp |\mathbf{p}|)}{32\pi}\left(2 + \frac{1}{z}\right) \times (1 - z)^2\theta(1 - z), \tag{C4}$$

$$\mathrm{Im}\sigma^\xi_{\pm,0}(|\mathbf{p}|, \omega; M) \equiv \mathrm{Im}\sigma^\xi_\pm(|\mathbf{p}|, \omega; M, T \to 0) = \frac{\mathrm{sgn}(\omega)(\omega \mp |\mathbf{p}|)}{32\pi}\frac{(1 - \xi z)^2}{z} \times \theta(1 - \xi z), \tag{C5}$$

where we have defined the dimensionless variable $z = M^2/p^2$.

In order to make a renormalization at zero temperature, we extract the *thermal* effect from the imaginary part of the self-energy,

$$\mathrm{Im}\sigma_{\pm,T}(|\mathbf{p}|, \omega; T, M) \equiv \mathrm{Im}\sigma_\pm(|\mathbf{p}|, \omega; T, M) - \mathrm{Im}\sigma_{\pm,0}(|\mathbf{p}|, \omega; M), \tag{C6}$$

and we calculate the real part of the thermal and vacuum effects separately. The former, $\mathrm{Re}\sigma_{\pm,T}$, is computed by using the Kramers-Kronig relation,

$$\mathrm{Re}\sigma_{\pm,T}(|\mathbf{p}|, \omega; T) = \mathcal{P}\int_{-\infty}^{\infty}\frac{d\omega'}{\pi}\frac{\mathrm{Im}\sigma_{\pm,T}(|\mathbf{p}|, \omega'; T)}{\omega' - \omega}. \tag{C7}$$

Here "$\mathcal{P}$" represents taking a Cauchy principal value in the integral. The renormalization at $T = 0$ can be manipulated by utilizing the (twice-) subtracted dispersion relation,

$$\mathrm{Re}\sigma_{\pm,0}(|\mathbf{p}|,\omega) = C_0 + C_1\cdot(\omega \mp |\mathbf{p}|) + (\omega \mp |\mathbf{p}|)^2 \cdot \mathcal{P}\int_{-\infty}^{\infty}\frac{d\omega'}{\pi}\frac{\mathrm{Im}\sigma_{\pm,0}^{\mathrm{U}+\xi}(|\mathbf{p}|,\omega')}{(\omega' \mp |\mathbf{p}|)^2(\omega'-\omega)}. \tag{C8}$$

The coefficients $C_{0,1}$ are determined to be zero by imposing on-shell renormalization conditions, $\sigma_{\pm,0}(|\mathbf{p}|,\omega)|_{\omega=\pm|\mathbf{p}|}=0$ and $\partial_\omega\sigma_{\pm,0}(|\mathbf{p}|,\omega)|_{\omega=\pm|\mathbf{p}|}=0$. The straightforward calculation leads to

$$\mathrm{Re}\sigma_{\pm,0}(|\mathbf{p}|,\omega) = \frac{\omega\mp|\mathbf{p}|}{32\pi^2}\Bigg[2z-(2+\xi)-\frac{(1-\xi z)^2}{z}\times\log\left|1-\frac{1}{\xi z}\right| + \left(2+\frac{1}{z}\right)(1-z)^2\times\log\left|1-\frac{1}{z}\right| - \frac{1}{z}\log\xi\Bigg], \tag{C9}$$

with $z = M^2/p^2$. The $\mathrm{Re}\sigma_{\pm,0}$ is regular in the limit $z\to\infty$ for any finite ξ.

Once we obtain $\mathrm{Im}\sigma_\pm$ and $\mathrm{Re}\sigma_\pm = \mathrm{Re}\sigma_{\pm,T} + \mathrm{Re}\sigma_{\pm,0}$ through the aforementioned procedures, the neutrino self-energy is now calculated by using Eq. (31),

$$\mathrm{Im}\Sigma_\pm^{(\nu)}(|\mathbf{p}|,\omega;T) = \left(\frac{g}{\sqrt{2}}\right)^2\mathrm{Im}\sigma_\pm(|\mathbf{p}|,\omega;T,M_{\mathrm{W}}(T)) + \left(\frac{g}{2\cos\theta_w}\right)^2\mathrm{Im}\sigma_\pm(|\mathbf{p}|,\omega;T,M_{\mathrm{Z}}(T)), \tag{C10}$$

$$\mathrm{Re}\Sigma_\pm^{(\nu)}(|\mathbf{p}|,\omega;T) = \left(\frac{g}{\sqrt{2}}\right)^2\mathrm{Re}\sigma_\pm(|\mathbf{p}|,\omega;T,M_{\mathrm{W}}(T)) + \left(\frac{g}{2\cos\theta_w}\right)^2\mathrm{Re}\sigma_\pm(|\mathbf{p}|,\omega;T,M_{\mathrm{Z}}(T)). \tag{C11}$$

Substituting these self-energies into Eq. (34), we obtain the neutrino spectral density $\rho_\pm^{(\nu)}(|\mathbf{p}|,\omega;T)$.

APPENDIX D: MASSLESS-HTL APPROXIMATION

We consider the limit $T\gg\omega,|\mathbf{p}|,M_{\mathrm{W,Z}}$ in the imaginary part of the self-energy [Eqs. (C1)–(C3)]. In both the unitary-gauge part [Eq. (C2)] and the ξ-dependent part [Eq. (C3)] the leading-order contributions are given by π^2T^2 terms in T^2J_{ST} [see Eq. (B11) for the expression of J_{ST}]. The total imaginary part of the self-energy in this limit reduces to

$$\mathrm{Im}\sigma_{\pm,\mathrm{HTL}}(|\mathbf{p}|,\omega;T) = \frac{\theta(-p^2)\pi T^2}{16|\mathbf{p}|^2}(\omega\mp|\mathbf{p}|). \tag{D1}$$

The real part is analytically evaluated through the Kramers-Kronig relation [Eq. (C7)], and reads

$$\mathrm{Re}\sigma_{\pm,\mathrm{HTL}}(|\mathbf{p}|,\omega;T) = \frac{T^2}{16|\mathbf{p}|^2}\left(2|\mathbf{p}| + (\omega\mp|\mathbf{p}|)\times\log\left|\frac{\omega-|\mathbf{p}|}{\omega+|\mathbf{p}|}\right|\right). \tag{D2}$$

Equations (D1) and (D2) correspond to well-known HTL results [1,2,12], and in this paper we call them "massless-HTL" approximations.

By using Eqs. (D1) and (D2), the neutrino self-energy in the massless HTL is given by

$$\mathrm{Im}\Sigma_{+,\mathrm{HTL}}^{(\nu)}(|\mathbf{p}|,\omega;T) = \left[\left(\frac{g}{\sqrt{2}}\right)^2+\left(\frac{g}{2\cos\theta_w}\right)^2\right]\mathrm{Im}\sigma_{+,\mathrm{HTL}}(|\mathbf{p}|,\omega;T), \tag{D3}$$

$$\mathrm{Re}\Sigma_{+,\mathrm{HTL}}^{(\nu)}(|\mathbf{p}|,\omega;T) = \left[\left(\frac{g}{\sqrt{2}}\right)^2+\left(\frac{g}{2\cos\theta_w}\right)^2\right]\mathrm{Re}\sigma_{+,\mathrm{HTL}}(|\mathbf{p}|,\omega;T). \tag{D4}$$

APPENDIX E: MASSIVE-HTL EXPANSION

We derive the HTL approximation which implements the massive weak-boson effects at high temperature ($M,\ T\gg\omega,\ |\mathbf{p}|$) for the fermion self-energy. We call this approximation the massive-HTL approximation, which reproduces the unitary-gauge HTL invented by Boyanovsky [15].

As explained in Appendix B, the one-loop momentum integral in the self-energy gives rise to the thermal integral factor $(I_{\mathrm{ST}},J_{\mathrm{ST}})$ given in Eqs. (B10) and (B11). The condition $M,\ T\gg\omega,\ |\mathbf{p}|$ allows us to divide their arguments $(x_\pm,y_\pm)$ into the dominant part $\zeta_\pm$ and the small perturbation part $\delta x_\pm,\delta y_\pm$,

$$x_\pm = \zeta_\pm + \delta x_\pm, \qquad y_\pm = \zeta_\pm + \delta y_\pm, \tag{E1}$$

$$\zeta_\pm = \frac{-M^2}{2T(\omega\pm|\mathbf{p}|)}, \tag{E2}$$

$$|\delta x_\pm| = \left|\frac{\omega\mp|\mathbf{p}|}{2T}\right| \ll 1, \qquad |\delta y_\pm| = \left|\frac{-\omega\mp|\mathbf{p}|}{2T}\right| \ll 1, \tag{E3}$$

$$|\zeta_\pm| \gg |\delta x_\pm|, \qquad |\delta y_\pm|. \tag{E4}$$

We expand the thermal integral factors $(I_{\mathrm{ST}},J_{\mathrm{ST}})$ in terms of $\delta x_\pm$. This massive-HTL expansion keeps the mass effects in the dominant part $\zeta_\pm$, in sharp contrast to the massless-HTL approximation.

We perform the massive-HTL expansion in the imaginary part of the self-energy [Eqs. (C2) and (C3)]. The leading contributions come from the unitary-gauge part and are found to be

$$\begin{aligned}&\mathrm{Im}\sigma_{\pm,\mathrm{MHTL}}(|\mathbf{p}|,\omega;T,M)\\&=\frac{\pm1}{16\pi|\mathbf{p}|^2}\Big[-TM^2\int_{\zeta_-}^{\zeta_+}d\zeta[N_\mathrm{F}(\zeta)+N_\mathrm{B}(\zeta)]\\&\quad-2T^2(\omega\mp|\mathbf{p}|)\int_{\zeta_-}^{\zeta_+}d\zeta\zeta[N_\mathrm{F}(\zeta)+N_\mathrm{B}(\zeta)]\\&\quad+\theta(-p^2)\cdot\pi^2T^2(\omega\mp|\mathbf{p}|)\Big].\end{aligned}\tag{E5}$$

We evaluate the leading effects of the real part by substituting the imaginary part [Eq. (E5)] into the Kramers-Kronig relation [Eq. (C7)],

$$\begin{aligned}&\mathrm{Re}\sigma_{\pm,\mathrm{MHTL}}(|\mathbf{p}|,\omega;T,M)\\&=\mathcal{P}\int_{-\infty}^{\infty}\frac{d\omega'}{\pi}\frac{\mathrm{Im}\sigma_{\pm,\mathrm{MHTL}}(|\mathbf{p}|,\omega';\mathrm{T},\mathrm{M})}{\omega'-\omega}\\&=\frac{\pm1}{16\pi^2|\mathbf{p}|^2}\int_{-\infty}^{\infty}d\omega'\sum_{s=\pm}s\sum_{\mathrm{D=F,B}}\\&\quad\times\left[TM^2\frac{I_\mathrm{D}[\zeta_s(\omega')]}{\omega'-\omega}+2T^2(\omega\mp|\mathbf{p}|)\frac{J_\mathrm{D}[\zeta_s(\omega')]}{\omega'-\omega}\right]\\&\quad\pm\int_{-\infty}^{\infty}d\omega'\frac{\theta(-p'^2)}{16\pi^2|\mathbf{p}|^2}\left[\pi^2T^2\frac{\omega'\mp|\mathbf{p}|}{\omega'-\omega}\right],\end{aligned}\tag{E6}$$

where we have defined

$$I_\mathrm{F,B}[\zeta_-]-I_\mathrm{F,B}[\zeta_+]\equiv\int_{\zeta_+}^{\zeta_-}dxN_\mathrm{F,B}(x),\tag{E7}$$

$$J_\mathrm{F,B}[\zeta_-]-J_\mathrm{F,B}[\zeta_+]\equiv\int_{\zeta_+}^{\zeta_-}dxxN_\mathrm{F,B}(x),\tag{E8}$$

$$\zeta_\pm=-\frac{M^2}{2T(\omega\mp|\mathbf{p}|)},\tag{E9}$$

with $p'^2=\omega'^2-|\mathbf{p}|^2$. We have omitted ω-independent terms, which cancel one another owing to the translation invariance of $\int_{-\infty}^{\infty}d\omega'$. We introduce the new integration measure $d\zeta=d(-M^2/(2T(\omega'+s|\mathbf{p}|)))$ with $s=\pm$, and evaluate the integral of statistical factors $I_\mathrm{D=F,B}$ involved in Eq. (E6) as

$$\begin{aligned}\int_{-\infty}^{\infty}d\omega'\frac{I_\mathrm{D=F,B}[\zeta_s(\omega')]}{\omega'-\omega}&=\int_{-\infty}^{\infty}\frac{d\zeta}{\zeta^2}\frac{M^2}{2T}\frac{I_\mathrm{D}[\zeta]}{-s|\mathbf{p}|-M^2/(2T\zeta)-\omega}\\&=\int_{-\infty}^{\infty}d\zeta I_\mathrm{D}[\zeta]\cdot\frac{d}{d\zeta}\log\left|\frac{\omega}{T}+s\frac{|\mathbf{p}|}{T}+\frac{M^2}{2T^2\zeta}\right|\\&=\int_{-\infty}^{\infty}d\zeta\frac{d}{d\zeta}[I_\mathrm{D}[\zeta]\cdot\log\left|\frac{\omega}{T}+s\frac{|\mathbf{p}|}{T}+\frac{M^2}{2T^2\zeta}\right|]-\int_{-\infty}^{\infty}d\zeta N_\mathrm{D}(\zeta)\cdot\log\left|\frac{\omega}{T}+s\frac{|\mathbf{p}|}{T}+\frac{M^2}{2T^2\zeta}\right|\\&=[I_\mathrm{D}[\infty]-I_\mathrm{D}[-\infty]]\log\left|\frac{\omega}{T}+s\frac{|\mathbf{p}|}{T}\right|-\sum_{t=\pm}\int_0^{\infty}d\zeta N_\mathrm{D}(t\zeta)\cdot\log\left|\frac{\omega}{T}+s\frac{|\mathbf{p}|}{T}+t\frac{M^2}{2T^2\zeta}\right|.\end{aligned}\tag{E10}$$

In the third equality, we have taken the partial derivative and used $dI_\mathrm{F,B}(\zeta)/d\zeta=N_\mathrm{F,B}(\zeta)$. Repeating the same procedure for the integral of $J_\mathrm{D=F,B}$ contained in Eq. (E6), we obtain

$$\begin{aligned}&\int_{-\infty}^{\infty}d\omega'\frac{J_\mathrm{D=F,B}[\zeta_s(\omega')]}{\omega'-\omega}\\&=[J_\mathrm{D}[\infty]-J_\mathrm{D}[-\infty]]\log\left|\frac{\omega}{T}+s\frac{|\mathbf{p}|}{T}\right|\\&\quad-\sum_{t=\pm}\int_0^{\infty}d\zeta t\zeta\cdot N_\mathrm{D}(t\zeta)\cdot\log\left|\frac{\omega}{T}+s\frac{|\mathbf{p}|}{T}+t\frac{M^2}{2T^2\zeta}\right|.\end{aligned}\tag{E11}$$

Here, we utilize the following formulas:

$$\sum_{\mathrm{D=F,B}}[I_\mathrm{D}[\infty]-I_\mathrm{D}[-\infty]]=\int_{-\infty}^{\infty}dx\left[\frac{1}{e^x+1}+\frac{1}{e^x-1}\right]=0,\tag{E12}$$

$$\sum_{\mathrm{D=F,B}}[J_\mathrm{D}[\infty]-J_\mathrm{D}[-\infty]]=\int_{-\infty}^{\infty}dx\left[\frac{x}{e^x+1}+\frac{x}{e^x-1}\right]=\frac{\pi^2}{2},\tag{E13}$$

$$\sum_{\mathrm{D=F,B}}N_\mathrm{D}(t\zeta)=t\frac{2e^{-\zeta}}{1-e^{-2\zeta}}.\tag{E14}$$

We then evaluate the summation $\sum_{t=\pm}$ in Eqs. (E10) and (E11) as

$$\begin{aligned}&\sum_{\mathrm{D=F,B}}\int_{-\infty}^{\infty}d\omega'\frac{I_\mathrm{D=F,B}[\zeta_s(\omega')]}{\omega'-\omega}\\&=-\int_0^{\infty}d\zeta\frac{2e^{-\zeta}}{1-e^{-2\zeta}}\log\left|\frac{\bar\omega+s|\bar{\mathbf{p}}|+\bar\Delta/\zeta}{\bar\omega+s|\bar{\mathbf{p}}|-\bar\Delta/\zeta}\right|,\end{aligned}\tag{E15}$$

$$\sum_{\mathrm{D=F,B}} \int_{-\infty}^{\infty} d\omega' \frac{J_{\mathrm{D=F,B}}[\zeta_s(\omega')]}{\omega' - \omega} = \frac{\pi^2}{2} \log \left| \frac{\omega}{T} + s\frac{|\mathbf{p}|}{T} \right| - \int_0^{\infty} d\zeta \frac{2\zeta e^{-\zeta}}{1 - e^{-2\zeta}} \times \log \left| \frac{\bar{\omega} + s|\bar{\mathbf{p}}| + \bar{\Delta}/\zeta}{\bar{\omega} + s|\bar{\mathbf{p}}| - \bar{\Delta}/\zeta} \right|, \quad \text{(E16)}$$

where we have defined $(\bar{\omega}, |\bar{\mathbf{p}}|) = (\omega/T, |\mathbf{p}|/T)$ and $\bar{\Delta} = M^2/(2T^2)$. Substituting Eqs. (E15) and (E16) into Eq. (E6), and performing $\sum_{s=\pm}$, we obtain the real part of the massive-HTL self-energy,

$$\mathrm{Re}\sigma_{\pm,\mathrm{MHTL}}(|\mathbf{p}|, \omega; T, M) = \frac{\pm T^2}{8|\mathbf{p}|} \pm \frac{1}{8\pi^2|\mathbf{p}|^2} \int_0^{\infty} d\zeta \frac{2\zeta e^{\zeta}}{1 - e^{-2\zeta}} \times \left[\left(2T^2(\omega \mp |\mathbf{p}|) - \frac{TM^2}{\zeta} \right) L_{\mathrm{P}}(\bar{\omega}, |\bar{\mathbf{p}}|, \bar{\Delta}/\zeta) + \left(2T^2(\omega \mp |\mathbf{p}|) + \frac{TM^2}{\zeta} \right) L_{\mathrm{M}}(\bar{\omega}, |\bar{\mathbf{p}}|, \bar{\Delta}/\zeta) \right], \quad \text{(E17)}$$

where

$$L_{\mathrm{P}}(\bar{\omega}, |\bar{\mathbf{p}}|, \bar{\Delta}/\zeta) = \frac{1}{2} \log \left| \frac{\bar{\omega} + |\bar{\mathbf{p}}| + \bar{\Delta}/\zeta}{\bar{\omega} + |\bar{\mathbf{p}}| - \bar{\Delta}/\zeta} \right|, \quad \text{(E18)}$$

$$L_{\mathrm{M}}(\bar{\omega}, |\bar{\mathbf{p}}|, \bar{\Delta}/\zeta) = \frac{1}{2} \log \left| \frac{\bar{\omega} - |\bar{\mathbf{p}}| + \bar{\Delta}/\zeta}{\bar{\omega} - |\bar{\mathbf{p}}| - \bar{\Delta}/\zeta} \right|, \quad \text{(E19)}$$

which is nothing but the formulas in the unitary gauge given in Ref. [15].

In summary, the neutrino self-energy in the leading order of the massive-HTL expansion is given by

$$\mathrm{Im}\Sigma^{(\nu)}_{+,\mathrm{MHTL}}(|\mathbf{p}|, \omega; T) = \left(\frac{g}{\sqrt{2}}\right)^2 \mathrm{Im}\sigma_{+,\mathrm{MHTL}}(|\mathbf{p}|, \omega; T, M_{\mathrm{W}}) + \left(\frac{g}{2\cos\theta_w}\right)^2 \mathrm{Im}\sigma_{+,\mathrm{MHTL}}(|\mathbf{p}|, \omega; T, M_{\mathrm{Z}}), \quad \text{(E20)}$$

$$\mathrm{Re}\Sigma^{(\nu)}_{+,\mathrm{MHTL}}(|\mathbf{p}|, \omega; T) = \left(\frac{g}{\sqrt{2}}\right)^2 \mathrm{Re}\sigma_{+,\mathrm{MHTL}}(|\mathbf{p}|, \omega; T, M_{\mathrm{W}}) + \left(\frac{g}{2\cos\theta_w}\right)^2 \mathrm{Re}\sigma_{+,\mathrm{MHTL}}(|\mathbf{p}|, \omega; T, M_{\mathrm{Z}}). \quad \text{(E21)}$$

APPENDIX F: SELF-ENERGY $\sigma_{\pm}$ WITH VANISHING GAUGE-BOSON MASS

We analytically evaluate the imaginary part of the self-energy at the one-loop level in the limit of vanishing gauge-boson masses ω, $|\mathbf{p}|$, $T \gg M \to 0$, and derive the expression (38).

The imaginary part of the self-energies [Eq. (C1)] can be rewritten as

$$\mathrm{Im}\sigma_{\pm}(|\mathbf{p}|, \omega; T, M(T)) = \frac{\pm 1}{32\pi|\mathbf{p}|^2} \left[\frac{-p^2}{M^2}(\omega \mp |\mathbf{p}|)^2 T \left[I_{\mathrm{ST}}\left(x_+, x_-; \frac{\omega}{T}\right) - I_{\mathrm{ST}}\left(x'_+, x'_-; \frac{\omega}{T}\right) \right] + (\omega \mp |\mathbf{p}|)^2 T \left[I_{\mathrm{ST}}\left(x_+, x_-; \frac{\omega}{T}\right) - \xi I_{\mathrm{ST}}\left(x'_+, x'_-; \frac{\omega}{T}\right) \right] - 2(-p^2 + M^2) T I_{\mathrm{ST}}\left(x_+, x_-; \frac{\omega}{T}\right) + 2\frac{p^2}{M^2}(\omega \mp |\mathbf{p}|) T^2 \left[J_{\mathrm{ST}}\left(x_+, x_-; \frac{\omega}{T}\right) - J_{\mathrm{ST}}\left(x'_+, x'_-; \frac{\omega}{T}\right) \right] - 4(\omega \mp |\mathbf{p}|) T^2 J_{\mathrm{ST}}\left(x_+, x_-; \frac{\omega}{T}\right) \right], \quad \text{(F1)}$$

where the statistical integral factors I_{ST} and J_{ST} are defined by Eqs. (B10) and (B11), respectively. The arguments of I_{ST} and J_{ST} are defined as

$$(x_{\pm}, x'_{\pm}) = \left(\frac{p^2 - M^2}{2T(\omega \pm |\mathbf{p}|)}, \frac{p^2 - \xi M^2}{2T(\omega \pm |\mathbf{p}|)} \right). \quad \text{(F2)}$$

In order to investigate the gauge boson–mass dependence of the self-energy (F1) in the limit $M \to 0$, we expand the integral factor $(I_{\mathrm{ST}}, J_{\mathrm{ST}})$ in terms of M^2 as

$$I_{\mathrm{ST}}(x_+, x_-) = I_{\mathrm{ST}}(X_+, X_-) - M^2 \sum_{s=\pm} Z_s [N_{\mathrm{F}}(X_s) + N_{\mathrm{B}}(Y_s)] + \mathcal{O}(M^4), \quad \text{(F3)}$$

$$J_{\mathrm{ST}}(x_+, x_-) = J_{\mathrm{ST}}(X_+, X_-) - M^2 \sum_{s=\pm} Z_s \left[X_s N_{\mathrm{F}}(X_s) + Y_s N_{\mathrm{B}}(Y_s) + \frac{\omega}{T} N_{\mathrm{B}}(Y_s) \right] + \mathcal{O}(M^4), \quad \text{(F4)}$$

where $x_{\pm} = X_{\pm} + M^2 Z_{\pm}$, and

$$(X_{\pm}, Y_{\pm}) = \left(\frac{\omega \mp |\mathbf{p}|}{2T}, \frac{-\omega \mp |\mathbf{p}|}{2T} \right), \quad \text{(F5)}$$

$$Z_{\pm} = \frac{1}{2T(\omega \pm |\mathbf{p}|)}. \quad \text{(F6)}$$

The M^2 expansions for the ξ-dependent sector $[I_{\rm ST}(x'_+, x'_-),\ J_{\rm ST}(x'_+, x'_-)]$ are obtained by replacing M^2 with ξM^2 in Eqs. (F3) and (F4).

It turns out that the leading terms $I_{\rm ST}(X_+, X_-)$ and $J_{\rm ST}(X_+, X_-)$ are common between the unitary-gauge and the ξ-dependent part. Owing to this property, all terms proportional to $1/M^2$ cancel out in Eq. (F1) and read

$$\begin{aligned}
&{\rm Im}\sigma_\pm(|\mathbf{p}|, \omega; T)|_{M\to 0} \\
&= \frac{\pm 1}{32\pi|\mathbf{p}|^2}\Big[((1-\xi)(\omega \mp |\mathbf{p}|)^2 + 2p^2) \\
&\quad \times T I_{\rm ST}\Big(X_+, X_-; \frac{\omega}{T}\Big) - 4(\omega \mp |\mathbf{p}|)T^2 J_{\rm ST} \\
&\quad \times \Big(X_+, X_-; \frac{\omega}{T}\Big) - T p^2(1-\xi)(\omega \mp |\mathbf{p}|) \\
&\quad \times \sum_{s=\pm} s Z_s H_\pm(X_s, Y_s)\Big], \qquad \text{(F7)}
\end{aligned}$$

where $H_\pm$ is defined as

$$\begin{aligned}
H_\pm(X_s, Y_s) &= (\omega \mp |\mathbf{p}|)[N_{\rm F}(X_s) + N_{\rm B}(Y_s)] - 2\omega N_{\rm B}(Y_s) \\
&\quad - 2T[X_s N_{\rm F}(X_s) + Y_s N_{\rm B}(Y_s)]. \qquad \text{(F8)}
\end{aligned}$$

Next, we simplify the final line of Eq. (F7). To this end, we explicitly evaluate $H_\pm(X_s, Y_s)$,

$$H_+(X_-, Y_-) = -2|\mathbf{p}|[N_{\rm F}(X_-) + N_{\rm B}(Y_-)], \qquad \text{(F9)}$$

$$H_-(X_+, Y_+) = 2|\mathbf{p}|[N_{\rm F}(X_+) + N_{\rm B}(Y_+)], \qquad \text{(F10)}$$

$$H_+(X_+, Y_+) = H_-(X_-, Y_-) = 0, \qquad \text{(F11)}$$

which enables us to perform the remaining summation $\sum_s$ in the final line of Eq. (F7) as

$$\sum_s s Z_s H_\pm(X_s, Y_s) = -2|\mathbf{p}| Z_\mp [N_{\rm F}(X_\mp) + N_{\rm B}(Y_\mp)] = -\frac{|\mathbf{p}|[N_{\rm F}(X_\mp) + N_{\rm B}(Y_\mp)]}{T(\omega \mp |\mathbf{p}|)}. \qquad \text{(F12)}$$

Substituting this expression for Eq. (F7), we obtain the desired expression (38) as the imaginary part of the self-energy with vanishing gauge-boson masses.

[1] M. Le Bellac, *Thermal Field Theory* (Cambridge University Press, Cambridge, England, 1996).

[2] J. I. Kapusta and C. Gale, *Finite-Temperature Field Theory, Principles and Applications* (Cambridge University Press, Cambridge, England, 2006).

[3] A. Pilaftsis, Phys. Rev. D **56**, 5431 (1997); Nucl. Phys. **B504**, 61 (1997); Phys. Rev. Lett. **95**, 081602 (2005); A. Pilaftsis and T. E. J. Underwood, Nucl. Phys. **B692**, 303 (2004); A. Pilaftsis, Phys. Rev. D **56**, 5431 (1997).

[4] A. Pilaftsis and T. E. J. Underwood, Phys. Rev. D **72**, 113001 (2005).

[5] M. Fukugita and T. Yanagida, Phys. Lett. B **174**, 45 (1986).

[6] For recent reviews, see for example W. Buchmuller, R. D. Peccei, and T. Yanagida, Annu. Rev. Nucl. Part. Sci. **55**, 311 (2005); C. S. Fong, M. C. Gonzalez-Garcia, and E. Nardi, Int. J. Mod. Phys. A **26**, 3491 (2011); S. Davidson, E. Nardi, and Y. Nir, Phys. Rep. **466**, 105 (2008); A. Pilaftsis, J. Phys. Conf. Ser. **171**, 012017 (2009).

[7] V. A. Kuzmin, V. A. Rubakov, and M. E. Shaposhnikov, Phys. Lett. **155B**, 36 (1985).

[8] F. R. Klinkhamer and N. S. Manton, Phys. Rev. D **30**, 2212 (1984).

[9] P. B. Arnold and L. D. McLerran, Phys. Rev. D **36**, 581 (1987).

[10] F. Englert and R. Brout, Phys. Rev. Lett. **13**, 321 (1964); P. W. Higgs, Phys. Lett. **12**, 132 (1964); G. S. Guralnik, C. R. Hagen, and T. W. B. Kibble, Phys. Rev. Lett. **13**, 585 (1964).

[11] V. V. Klimov, Yad. Fiz. **33**, 1734 (1981) [Sov. J. Nucl. Phys. **33**, 934 (1981)]; H. A. Weldon, Phys. Rev. D **40**, 2410 (1989); **26**, 2789 (1982); **26**, 1394 (1982).

[12] R. D. Pisarski, Phys. Rev. Lett. **63**, 1129 (1989); E. Braaten and R. D. Pisarski, Nucl. Phys. **B337**, 569 (1990); **B339**, 310 (1990); J. Frenkel and J. C. Taylor, Nucl. Phys. **B334**, 199 (1990).

[13] G. Baym, J. P. Blaizot, and B. Svetitsky, Phys. Rev. D **46**, 4043 (1992).

[14] J. C. D'Olivo, J. F. Nieves, and M. Torres, Phys. Rev. D **46**, 1172 (1992).

[15] D. Boyanovsky, Phys. Rev. D **72**, 033004 (2005).

[16] M. Kitazawa, T. Kunihiro, and Y. Nemoto, Phys. Lett. B **633**, 269 (2006); Prog. Theor. Phys. **117**, 103 (2007).

[17] M. Kitazawa, T. Kunihiro, K. Mitsutani, and Y. Nemoto, Phys. Rev. D **77**, 045034 (2008).

[18] D. Satow, Y. Hidaka, and T. Kunihiro, Phys. Rev. D **83**, 045017 (2011).

[19] E. C. G. Stueckelberg, Helv. Phys. Acta **11**, 225 (1938); **11**, 299 (1938); **11**, 312 (1938).

[20] For a review article, see H. Ruegg and M. Ruiz-Altaba, Int. J. Mod. Phys. A **19**, 3265 (2004).

[21] M. Harada and Y. Nemoto, Phys. Rev. D **78**, 014004 (2008); M. Harada, Y. Nemoto, and S. Yoshimoto, Prog. Theor. Phys. **119**, 117 (2008).

[22] S. x. Qin, L. Chang, Y. x. Liu, and C. D. Roberts, Phys. Rev. D **84**, 014017 (2011).
[23] H. Nakkagawa, H. Yokota, and K. Yoshida, Phys. Rev. D **85**, 031902 (2012); **86**, 096007 (2012).
[24] K. Fujikawa, B. W. Lee, and A. I. Sanda, Phys. Rev. D **6**, 2923 (1972).
[25] C. Manuel, Phys. Rev. D **58**, 016001 (1998).
[26] K. Kajantie, M. Laine, K. Rummukainen, and M. E. Shaposhnikov, Phys. Rev. Lett. **77**, 2887 (1996); F. Csikor, Z. Fodor, P. Hegedus, A. Jakovac, S. D. Katz, and A. Piroth, Phys. Rev. Lett. **85**, 932 (2000); Y. Aoki, F. Csikor, Z. Fodor, and A. Ukawa, Phys. Rev. D **60**, 013001 (1999); F. Csikor, Z. Fodor, and J. Heitger, Nucl. Phys. B Proc. Suppl. **73**, 659 (1999); Phys. Rev. Lett. **82**, 21 (1999).
[27] S. Chatrchyan *et al.* (CMS Collaboration), Phys. Lett. B **716**, 30 (2012).
[28] G. Aad *et al.* (ATLAS Collaboration), Phys. Lett. B **716**, 1 (2012).
[29] T. Aaltonen *et al.* (CDF Collaboration), Phys. Rev. Lett. **109**, 111802 (2012).
[30] V. M. Abazov *et al.* (D0 Collaboration), Phys. Rev. Lett. **109**, 121802 (2012).
[31] V. A. Rubakov and M. E. Shaposhnikov, Usp. Fiz. Nauk **166**, 493 (1996) [Phys. Usp. **39**, 461 (1996)].
[32] V. V. Lebedev and A. V. Smilga, Ann. Phys. (N.Y.) **202**, 229 (1990); Y. Hidaka, D. Satow, and T. Kunihiro, Nucl. Phys. **A876**, 93 (2012).
[33] For a recent review, see, M. Drewes, Int. J. Mod. Phys. E **22**, 1330019 (2013).
[34] A. Anisimov, W. Buchmuller, M. Drewes, and S. Mendizabal, Phys. Rev. Lett. **104**, 121102 (2010); Ann. Phys. (Amsterdam) **326**, 1998 (2011).
[35] C. P. Kiessig, M. Plumacher, and M. H. Thoma, Phys. Rev. D **82**, 036007 (2010); C. Kiessig and M. Plumacher, J. Cosmol. Astropart. Phys. 07 (2012) 014; 09 (2012) 012.
[36] D. Besak and D. Bodeker, J. Cosmol. Astropart. Phys. 03 (2012) 029.
[37] A. Anisimov, D. Besak, and D. Bodeker, J. Cosmol. Astropart. Phys. 03 (2011) 042.
[38] B. Garbrecht, F. Glowna, and M. Herranen, J. High Energy Phys. 04 (2013) 099; B. Garbrecht, F. Glowna, and P. Schwaller, arXiv:1303.5498.
[39] M. Laine, J. High Energy Phys. 05 (2013) 083.
[40] M. Drewes and B. Garbrecht, J. High Energy Phys. 03 (2013) 096.
[41] L. Carson, X. Li, L. D. McLerran, and R. T. Wang, Phys. Rev. D **42**, 2127 (1990); J. Baacke and S. Junker, Phys. Rev. D **50**, 4227 (1994); **49**, 2055 (1994).